A Spectral Line Survey of Selected 3 mm bands Toward Sagittarius B2(N-LMH) Using the NRAO 12 Meter Radio Telescope and the BIMA Array I. The Observational Data

D. N. Friedel[1], L. E. Snyder[1], B. E. Turner[2]

and

A. Remijan[1]

ABSTRACT

We have initiated a spectral line survey, at a wavelength of 3 millimeters, toward the hot molecular core Sagittarius B2(N-LMH). This is the first spectral line survey of the Sgr B2(N) region utilizing data from both an interferometer (BIMA Array) and a single-element radio telescope (NRAO 12 meter). In this survey, covering 3.6 GHz in bandwidth, we detected 218 lines (97 identified molecular transitions, 1 recombination line, and 120 unidentified transitions). This yields a spectral line density (lines per 100 MHz) of 6.06, which is much larger than any previous 3 mm line survey. We also present maps from the BIMA Array that indicate that most highly saturated species (3 or more H atoms) are products of grain chemistry or warm gas phase chemistry. Due to the nature of this survey we are able to probe each spectral line on multiple spatial scales, yielding information that could not be obtained by either instrument alone.

Subject headings: ISM: molecules — ISM:individual(Sgr B2) — Surveys — Radio Lines:ISM

1. Introduction

Sagittarius B2 is a massive star forming region at a distance of 7.1 kpc and within 300 pc of the Galactic center (Reid et al. 1988). It is well known for its abundance of molecular species and has been the target of many searches for complex molecules (e.g., Mehringer et al. 1997; Liu, Mehringer, & Snyder 2001; Martín-Pintado et al. 2001) and several spectral line surveys (e.g., Cummins, Thaddeus, & Linke 1986; Turner 1989, 1991). The region is made up of several individual sources. Table 1 contains a list of the main sources in the region along with their coordinates. The first column gives the source name. The second and third columns give the right ascension and declination of each source, respectively. The dense molecular core toward Sgr B2(N) has been called the "Large Molecule Heimat" (Sgr B2(N-LMH)) since it is the source of all of the large molecules observed in that region (Snyder, Kuan, & Miao 1994; Mehringer et al. 1997). Sgr B2(N-LMH) has the most detected and identified molecular species and has the strongest

[1]Department of Astronomy, University of Illinois, Urbana, IL 61801
email: friedel@astro.uiuc.edu, snyder@astro.uiuc.edu, aremijan@astro.uiuc.edu

[2]National Radio Astronomy Observatory, Charlottesville, VA 22903
email: bturner@nrao.edu

spectral emission lines of any source in the complex.[3] Within the 3 mm synthesized beam of the Berkeley-Illinois-Maryland Association (BIMA) Array[4] in its C configuration toward Sgr B2(N) there are at least four HII regions (de Pree et al. 1995). This is unlike Sgr B2(M), which has over 21 HII regions in the same size beam (Gaume et al. 1995; de Pree et al. 1996).

Spectral line surveys provide powerful tools to analyze the coupled dynamical and chemical evolution of molecular clouds. In a survey, many lines of a single species are observed at similar sensitivities, diminishing the errors associated with derived quantities. For example, a particular problem arises in deriving accurate abundances due to overlapping identifications of molecular species. Surveys provide the best means of avoiding this problem by revealing intensity changes in lines of a given species. The first line surveys of the Sgr B2 source complex were aimed at Sgr B2(OH). Sgr B2(OH) is an OH and H_2O maser source ($\sim 30''$ south of Sgr B2(M)), which is not a main site of molecular concentration in the region (Snyder, Kuan, & Pratap 1991) and furthermore has little or no millimeter continuum emission ($\leq$0.1 Jy beam^{-1}) (Kuan & Snyder 1994; Kuan, Mehringer, & Snyder 1996). However, the main beams of these surveys were large enough to encompass Sgr B2(M) and in the case of Cummins, Thaddeus, & Linke (1986), possibly even Sgr B2(N) at some frequencies. Thus, many of the molecular transitions detected by these surveys may not have come from Sgr B2(OH) but from Sgr B2(M) or Sgr B2(N). More recent surveys covering 330-355 GHz (Sutton et al. 1991) and 218-263 GHz (Nummelin et al. 1998, 2000) did use Sgr B2(N) and Sgr B2(M) as the primary sources. Figure 1 shows the pointing centers and average beams from this and previous spectral line surveys of the Sgr B2 region. The five cores of Sgr B2 are labeled (North, Northwest, Main, South, and OH). The beams from this survey are in bold face centered on Sgr B2(N). The dashed beams around Sgr B2(N), Sgr B2(M), and Sgr B2(NW) are from Nummelin et al. (1998, 2000). The grey beams around Sgr B2(N) and Sgr B2(M) (2 beams) are from Sutton et al. (1991). The beams centered on Sgr B2(OH) are from Turner (1989, 1991) and Cummins, Thaddeus, & Linke (1986).

This survey uses both the BIMA Array (ten 6.1 meter elements) and the single-element NRAO 12 meter[5] radio telescope. Unlike previous surveys that only used single-element telescopes, we are able to sample several spatial scales of this source. A single-element telescope is best for detecting large scale, extended emission, but poor at detecting compact sources due to beam dilution. An array is insensitive to structures larger than an angular size determined by the minimum spacing of its elements, and thus resolves out large scale structure. For the BIMA Array, this is $\sim$10 times the size of the synthesized beam (Wright 1996)[6]. This feature is very important in astrochemistry because the location of a particular molecular species may indicate its formation mechanism. Molecules formed by low temperature gas phase reactions will be primarily extended in emission. On the other hand, molecules formed on grains, while they may form anywhere in the cloud, will evaporate from the grains and be detected in the warmer compact cores of the sources (Caselli, Hasegawa, & Herbst 1993). Similarly, molecules formed by warm temperature gas phase reactions will also be detected in the warmer cores. Thus, a single element telescope would be most sensitive to molecules formed in extended low temperature gas clouds, while an array would be most sensitive to molecules formed in warm cores (either in warm gas phase reactions or initially on a grain and then desorbed from the surface).

---

[3]With the exception of SO and SO_2 which are strongest toward Sgr B2(M) (Sutton et al. 1991).

[4]Operated by the University of California, Berkeley, the University of Illinois, and the University of Maryland with support from the National Science Foundation.

[5]The National Radio Astronomy Observatory is a facility of the National Science Foundation operated under cooperative agreement by Associated Universities, Inc.

[6]BIMA Memoranda Series (Wright 1996) is available at: http://bima.astro.umd.edu/memo/memo45.ps.

Our spectral line survey is the first to use both interferometric data and single-element telescope data from Sgr B2(N-LMH) and is also the first 3 mm survey of this source. Here we present the results of a line survey towards Sgr B2(N-LMH) of six 600 MHz wide spectral bands (Figure 2). All bands were observed with both the BIMA Array and the NRAO 12 meter radio telescope.

2. Observations and Data

The pointing center of our survey was Sgr B2(N-LMH)[7]. The spectral bands surveyed (Figure 2) were centered on 86.2, 86.8, 90.025, 106.58, 108.5 and 110.2 GHz.[8] We chose these bands because each contains at least one previously identified molecular transition. In most cases, the spectral bands contained many well known molecular species including silicon monoxide (SiO), sulfur monoxide (SO), deuterated ammonia (NH_2D), methyl formate ($HCOOCH_3$, MeF), cyanogen (^{13}CN), carbon monoxide (^{13}CO), methyl cyanide (CH_3CN) and formamide (NH_2CHO).

2.1. NRAO 12 Meter Telescope Observations

The NRAO 12 meter telescope observations were carried out in 2000 July. The spectra observed with the 12 meter telescope utilized the dual-channel SIS mixer receiver operating in a single-sideband mode with the image sideband rejected at a typical level of 20 dB. The MAC spectrometer was used in its 600 MHz bandwidth mode with a channel spacing of 195 kHz per channel. This gives a frequency resolution of 391 kHz per channel, owing to internal Hanning weighting, and a velocity resolution of ∼1.4, 1.4, 1.3, 1.1, 1.1 and 1.1 km s^{-1} for the 86.2, 86.8, 90.025, 106.58, 108.5 and 110.2 GHz bands. The two receivers provided orthogonal linear polarizations and integrated on source for 1.75-2.5 hours. Calibration of the intensity scale made use of the chopper wheel method, with the resulting data on the T_A^* scale. This was converted to the T_R^* scale by applying the main beam efficiency, which varies between 0.68 at 86 GHz and 0.62 at 110 GHz, and is accurate to within ∼5% (Kutner & Ulich 1981). This scale corrects for atmospheric extinction and telescope spillover losses, but not for error-beam losses or the forward beam coupling to the source. Data were taken using position switching with the reference position 30′ west in azimuth in order to avoid any extended structure. The passbands were calibrated by baseline fitting to the data with a polynomial of order 4 or less. The passbands were checked before and after calibration for spurious features; none were found. The 12 meter telescope data were analyzed with the UniPOPS software package (Salter, Maddalena, & Garwood 1995)[9].

2.2. BIMA Array Observations

Observations with the BIMA Array were carried out in C configuration (minimum baseline of 8 meters and maximum baseline of 61 meters) between 2001 March and 2002 April. The array was operating in

[7]While this is the pointing center of all observations, the beams of both telescopes also encompassed other sources within Sgr B2(N).

[8]While the BIMA Array observed a wider spectral band than the 12 meter telescope in several instances, these data are not being presented in this paper since there is not 12 meter data to compare it to, but will be presented in future papers.

[9]UniPOPS information is available at: http://info.gb.nrao.edu/∼rmaddale/140ft/unipops/unipops_toc.html.

cross-correlation mode (double sideband) with a sideband rejection of better than 20 dB. The correlator configuration was four 50 MHz spectral windows set side by side with the edges overlapping by 3 channels, giving an effective bandwidth of just under 200 MHz in each sideband. Each window had 128 channels resulting in a spectral resolution of 390 kHz per channel and a velocity resolution of ∼1.4, 1.4, 1.3, 1.1, 1.1 and 1.1 km s^{-1} for the 86.2, 86.8, 90.025, 106.58, 108.5 and 110.2 GHz bands. This set of 4 windows was set up to start at the lower end of each of the 600 MHz wide spectral bands and integrated on source for 50 minutes. Next, the observing frequency was shifted by 197 MHz and the integration was continued. This process was repeated until the entire 600 MHz band was observed. Neptune and Mars were used as flux density calibrators and 1733-130 was used to calibrate the antenna based gains. The absolute amplitude calibration of 1733-130 from the flux density calibrators is accurate to within ∼20%. The passbands were automatically calibrated online during data acquisition.[10] In the past this method has been quite satisfactory and has not generated spurious features. The BIMA Array data were calibrated and imaged using the MIRIAD software package (Sault, Teuben, & Wright 1995).

2.3. Data

Table 2 contains a list of beam sizes and rms noise levels for the observations. The first column lists the central frequency of the observed band (GHz). The second and third columns list the synthesized beam size (arcsec) and the 1σ channel rms noise level (Jy beam^{-1}) for the BIMA Array observations, which have been averaged over all windows. The last two columns list the FWHM beam size (arcsec) and the 1σ channel rms noise level (Jy beam^{-1}) of the 12 meter telescope observations. The 1σ rms noise levels from the BIMA Array were determined by taking the rms over all channels from a spatial region that was free from continuum emission. The 1σ rms noise levels from the 12 meter telescope were determined by calculating the rms in sections of line free channels.

The spectra are presented in Figures 3(a-l). In order to derive the frequency scale for the BIMA Array, V_{LSR}=64 km s^{-1} was used (Mehringer et al. 1997). For the 12 meter telescope V_{LSR}=65 km s^{-1} was used because it is the value in a standard 12 meter catalog. In the figures, the two upper panels show BIMA Array data, and the bottom panel shows 12 meter telescope data. The top panel in each figure shows BIMA Array data which are Hanning weighted to bring out weaker features by reducing the noise level. The middle panel in each figure shows the BIMA Array data which are unsmoothed (not Hanning weighted) in order to preserve narrow features which are also seen in the 12 meter telescope data. The 12 meter telescope data were automatically Hanning smoothed as part of the internal data acquisition routine. The spectral resolution of the unsmoothed BIMA Array data match that of the smoothed 12 meter telescope data to within 1 kHz. The 12 meter telescope intensity scale was converted from T_R^* to Jy beam^{-1} using 30.5, 30.6, 30.8, 31.6, 31.8, 32.0 Jy K^{-1} as conversion factors for the 86.2, 86.8, 90.025, 106.58, 108.5 and 110.2 GHz bands, respectively. The dashed lines on the BIMA Array spectra denote spectral window edges and the "I" bars, in both the 12 meter telescope and BIMA Array data (unsmoothed), denote 1σ rms noise levels. The threshold for defining a line is as follows: it must have a signal-to-noise of at least 3σ and have a line width of at least 4 km s^{-1} (unless a notable feature is seen at the same frequency with both instruments). Unidentified lines labeled with "Q" are questionable detections due to their narrow line width.

Table 3 summarizes the molecular detections of the survey. The first column lists the molecule; the

[10]A technical description of this can be found at: http://astron.berkeley.edu/∼plambeck/technical.html.

second and third columns list the number of detected transitions by the BIMA Array and the 12 meter telescope, respectively. The fourth column lists the reference for the molecular information for each species. Table 4 lists the molecular transitions grouped by molecule. The first column lists the rest frequency of the transition, along with the 2σ standard deviation. The second column lists the quantum numbers of the transition. The third and fourth columns list the intensity and line width[11], with the 2σ standard deviation, of each line observed by the BIMA Array. Fits to the BIMA Array data were on the unsmoothed spectra. If the transition was not detected, a 1σ upper limit has been set for the intensity. The fifth and sixth columns list the intensity and line width, with the 2σ standard deviation, of each line observed by the 12 meter telescope. In a single case from the BIMA Array, the blend of MeF and NH_2D at 85.92 GHz (see Figure 3a), the MeF lines were modeled using the fits to the other detected MeF transitions, in order to obtain a satisfactory fit to all components. The seventh column lists the upper energy level of each transition. The eighth column lists the product of the line strength and the square of the relevant dipole moment. Table 5 lists the detected unidentified (U) lines. The first column lists the rest frequency (based on the LSR velocity of Sgr B2(N-LMH)). The second and third columns list the peak intensity and line width, with the 2σ standard deviation, of each line from the BIMA Array. The fourth and fifth columns list the peak intensity and line width, with the 2σ standard deviation, of each line from the 12 meter telescope. If a line was undetected by one of the telescopes, a 1σ upper limit has been set for the intensity. In order to find potential identifications for the U lines, we searched the JPL database (Pickett et al. 1998), The Cologne Database for Molecular Spectroscopy (Müller et al. 2001), and the Lovas List, a compilation of observed molecular transitions from the ISM (Lovas 2004). Potential identifications were also given by F. J. Lovas (private communication, hereafter FJL) and J. C. Pearson (private communication, hereafter JCP). The sixth column gives these potential identifications, which were made based on the rest frequency of the transition. Any transition having a 2σ frequency standard deviation greater than 1 MHz (3 km s^{-1} at 3 mm) or any molecule containing astrophysically unlikely elements was excluded. Three of these transitions are labeled as potentially coming from NH_2CH_2COOH-I (glycine), although the likelihood of this identification is small (an explanation is given with each label). There are 21 U lines listed in Table 5 (denoted with footnote *a*) which do not meet both of the threshold criteria, 15 from the BIMA Array and 6 from the 12 meter telescope. While the origin of these lines is unknown, those detected by the BIMA Array are most likely coming from the warmest and most compact parts of the core and could be vibrationally excited transitions of unidentified species. Those detected by the 12 meter telescope are most likely coming from the extended cool gas around the core. These lines are not included in any of the line counts or statistics.

3. Results

3.1. Statistics

In this survey, we detected a total of 218 lines (97 identified molecular transitions from 18 molecular species and 16 isotopomers, 1 recombination line, and 120 U lines). The BIMA Array detected 199 lines (91 from 15 molecular species and 16 isotopomers, and 108 U lines) and the 12 meter telescope detected 116 lines (74 from 17 molecular species and 15 isotopomers, 1 recombination line, and 41 U lines). Note that the number of detected lines does not include hyperfine transitions. Of the lines detected by the BIMA Array, 21 are previously undetected transitions of known molecules, 102 are previously undetected U lines, and 101 (23 transitions of known molecules and 79 U lines) were only detected by the BIMA Array. The 12

[11]Intensities and line widths were obtained by a Gaussian least squares fit to the line profiles.

meter telescope detected 12 previously undetected transitions of known molecules, 37 new U lines, and 19 (7 transitions of known molecules and 12 U lines) were only detected by the 12 meter telescope.

The above line counts yield a spectral line density (average number of lines per 100 MHz) of 6.06 from all observed lines (2.72 from identified lines and 3.34 from U lines). This is a large increase over previous 3 mm surveys of the Sgr B2 region. Table 6 compares the line counts and densities from this survey to previous 3 mm surveys of this source and from Lovas (2004). The first column gives the source of the data. The second and third columns give the line counts and densities (from the same frequency bands covered in this survey) of identified transitions from each source. The fourth and fifth columns give the line counts and density of U lines from each source. The sixth and seventh columns give the total line counts and densities from each source. The total line density from this survey is greater than from either of the previous line surveys and from Lovas (2004). The largest increase is the number of U lines detected; a total of ∼55% of the lines we detected are unidentified. This demonstrates that with higher sensitivity and smaller beams, more spectral features will be detected.

Due to the relatively large line widths (typically 5-10 km s^{-1}) and the large number of molecular species in the region, many spectral features are unresolved. In cases of very strong emission from a single transition, nearby weaker transitions may not have been observed. Thus if a specific transition was not detected, it may either currently lie below our detection limit or may be blended in the wings of stronger lines.

3.2. Maps

Figure 4 shows maps from the BIMA Array toward Sgr B2(N-LMH) of NH_2CHO (formamide), C_2H_5OH (ethanol, EtOH), SO, and $H^{13}CN$. In each map, the continuum is mapped in grey scale with the transition averaged over the FWHM of the line mapped in contours. The central continuum peak is Sgr B2(N) and the lower continuum peak is Sgr B2(M). The BIMA Array and 12 meter telescope spectra of each mapped transition are below their respective map. The vertical axis is intensity in Jy $beam^{-1}$ and the horizontal axis is frequency in GHz. The synthesized beam is given in the lower left corner of each map. The numbers on the grey scale wedge are in units of Jy $beam^{-1}$.

4. Discussion

The higher (>90 K) upper state energy (E_u) transitions of all species will map toward the core since these transitions are only populated to detectable levels in the warmer temperature regions. But the lower E_u transitions can be excited in both the warm core and the cooler surrounding gas. Thus, the lower E_u transitions trace a truer distribution of each molecular species and are an indicator of that molecule's formation mechanism. Since hydrogenation of atoms heavier than H and molecules happens with very high efficiency on grains (Watson & Salpeter 1972), all transitions of highly saturated (3 or more H atoms) molecules should map toward the core where the molecules are desorbing from the grain surfaces. Similarly, any molecule formed by reactions by ions or other heavier atoms and molecules on grain surfaces should map toward the core. We also expect any molecules formed in warm gas phase reactions will map primarily toward the hot core since this is where the temperatures are warm enough for the reactions to proceed. The lower E_u transitions of species which are produced by cool gas phase reactions should have a large extended component in their distribution, since these reactions do not require the higher temperatures of the core to proceed.

Figure 4(a) shows the BIMA Array map of the 106.541 GHz, $5_{2,3}$-$4_{2,2}$ transition of NH_2CHO which has an E_u=27.2 K. The contours are 3, 6, 9, 12, 15, 18, and 21σ. The average (across the FWHM of the line) flux detected by the BIMA Array is 6.27(29)[12] Jy beam^{-1} while the average flux detected by the 12 meter telescope is 8.61(63) Jy beam^{-1}. This map and the difference in flux indicate that NH_2CHO has a compact distribution toward the core with few extended components and most likely is the product of grain chemistry or warm gas phase chemistry. The observations by Schilke et al. (1991) agree with this view of the NH_2CHO distribution. With a 17″ beam they found unresolved NH_2CHO emission toward Sgr B2(N) with much weaker emission toward the Sgr B2(M) region. This map is indicative of most of the highly saturated species we have observed.

One of the exceptions is shown in Figure 4(b), which is the BIMA Array map of the 90.117 GHz, $4_{1,4}$-$3_{0,3}$ transition of EtOH with an E_u=9.4 K. The contours are -2, -1, 1, 3, and 4.5σ. This transition has peaks and valleys throughout the map and has an average flux of 0.60(15) Jy beam^{-1} from the BIMA Array and 8.20(68) Jy beam^{-1} from the 12 meter telescope. The 12 meter telescope spectrum has a much wider line as well as several more velocity components than the BIMA Array spectrum. This indicates that EtOH has a highly extended distribution and suggests a cooler gas phase formation mechanism. The 106.775 GHz, $9_{1,8}$-$8_{2,7}$ AA (E_u=43.4 K) transition of $(CH_3)_2O$ (dimethyl ether) (see Figure 3h), the other exception, maps similarly to this transition of EtOH. While there is no great intensity difference between the BIMA Array spectrum and 12 meter telescope spectrum of this transition, the 12 meter telescope spectrum has wider lines and several velocity components, indicating an extended distribution and a cool gas phase formation mechanism.

Figure 4(c) shows the BIMA Array map of the 86.093 GHz, 2_2-1_1 transition of SO which has an E_u=19.3 K. The contours are -6, -3, 3, 6, 9, 12, 15, 18, 21, and 24σ. The average flux detected by the BIMA Array is 6.69(28) Jy beam^{-1} and the average flux detected by the 12 meter telescope is 16.30(61) Jy beam^{-1}. This transition show the distinction between sulfurated species and highly saturated organic species in the region. It has strong peaks toward both Sgr B2(N-LMH) and Sgr B2(M) as well as strong peaks and valleys throughout the rest of the map. While most of the flux is coming from the hot core regions the flux difference between the two instruments along with the map indicated that SO has significant extended structure.

Figure 4(d) shows the BIMA Array map of the 86.340 GHz, $1_{0,1}$-$0_{0,0}$ transition of $H^{13}CN$ which has an E_u=4.0 K. The contours are -14, -12, -9, -6, -3, and 3σ. The map of this transition is indicative of the other species which also show strong absorption. This map, across the FWHM of the absorption, does not show any of the emission components seen in the 12 meter telescope spectrum. This is because these components are very extended and are being resolved out by the BIMA Array.

These maps show that the highly saturated species[13] such as EtCN, CH_3CN, MeF, NH_2CHO, and VyCN map toward the Sgr B2(N-LMH) core, indicating that these species are products of grain or warm gas phase chemistry. Contrasting this, two other highly saturated species, EtOH and $(CH_3)_2O$, show highly extended distributions, indicating a cooler gas phase formation mechanism.

---

[12]Errors quoted are 1σ rms noise level for the associated transition.

[13]No conclusion about the spatial distribution of CH_3OH can be made from our data since both detected transitions have a higher E_u of 102 K.

5. Summary

We have presented the spectra and line fits from the first 3 mm spectral line survey using both an interferometer and a single element radio telescope of the Sgr B2(N-LMH) hot molecular core. We detected 218 lines (97 identified molecular transitions from 18 molecular species and 16 isotopomers, 1 recombination line, and 120 unidentified transitions). The survey has a spectral line density of 6.06 lines per 100 MHz from all observed lines (2.72 from identified lines and 3.34 from U lines) which is much greater than any previous 3 mm survey of this source. The high density of U lines we detected (∼55% of all detected lines) indicates that as Sgr B2(N-LMH) is observed with increasing sensitivity and smaller beams, more spectral features will be seen.

Due to the nature of this survey we are able to probe each spectral line on multiple spatial scales, yielding information that could not be obtained by either instrument alone. From this spatial information we can constrain potential formation mechanisms for the identified molecular species. Products of cool gas phase reactions will show extended distributions while products of warm gas phase reactions or grain surface reactions will show compact distributions. The BIMA Array maps show that the observed highly saturated species such as EtCN, CH_3CN, MeF, NH_2CHO, and VyCN show compact emission from the Sgr B2(N-LMH) core, indicating a grain chemistry or warm gas phase chemistry formation mechanism. Contrasting this, two other highly saturated species, EtOH and $(CH_3)_2O$, show very extended distributions, indicating a cooler gas phase chemistry formation mechanism. A detailed analysis of selected data sets, including temperature determinations, column densities, and comparison of results with existing chemical models will be presented in a subsequent paper.

We thank D. S. Meier for many helpful discussions. F. J. Lovas, J. C. Pearson, and J. M. Hollis helped us identify U lines. We thank A. Apponi for help with information on the 12 meter telescope and J. R. Forster for help with information on the BIMA Array. We also thank an anonymous referee for many helpful comments which improved this manuscript. We acknowledge support from the Laboratory for Astronomical Imaging at the University of Illinois, NSF AST 99-81363, and NSF AST 02-28953.

REFERENCES

Bester, M., Yamada, K., Winnewisser, G., & Urban, S. 1983, A&A, 121, L13

Bogey, M., Demuynck, C., & Destombles, J. L. 1984, Canadian Journal of Physics, 62, 1248

Boucher, D., Burie, J., Bauer, A., Dubrulle, A., & Demaison, J. 1980, J. Phys. Chem. Ref. Data, 9, 659

Caselli, P., Hasegawa, T. I., & Herbst, E. 1993, ApJ, 408, 548

Cummins, S. E., Thaddeus, P., & Linke, R. A. 1986, ApJS, 60, 819

de Pree, C. G., Gaume, R. A., Goss, W. M., & Claussen, M. J. 1995, ApJ, 451, 284

de Pree, C. G., Gaume, R. A., Goss, W. M., & Claussen, M. J. 1996, ApJ, 464, 788

Frerking, M. A., Wilson, R. W., & Langer, W. D. 1979, ApJ, 232, L65

Gaume, R. A., Claussen, M. J., de Pree, C. G., Goss, W. M., & Mehringer, D. M. 1995, ApJ, 449, 663

Gerry, M. C. L., Yamada, K., & Winnewisser, G. 1979, J. Phys. Chem. Ref. Data, 8, 107

Gottlieb, C. A., Gottlieb, E. W., Thaddeus, P. & Vrtilek, J. M. 1986, ApJ, 303, 446

Groner, P., Albert, S., Herbst, E., & de Lucia, F. C. 1998, ApJ, 500, 1059

Groner, P., Albert, S., Herbst, E., De Lucia, F. C., Lovas, F. J., Drouin, B. J., & Pearson, J. C. 2002, ApJS, 142, 145

Guelin, M., Cernicharo, J., & Linke, R. A. 1982, ApJ, 263, L89

Johnson, D. R., Lovas, F. J., & Kirchhoff, W. H. 1972, J. Phys. Chem. Ref. Data, 1, 1011

Kuan, Y. & Snyder, L. E. 1994, ApJS, 94, 651

Kuan, Y., Mehringer, D. M., & Snyder, L. E. 1996, ApJ, 459, 619

Kutner, M. L. & Ulich, B. L. 1981, ApJ, 250, 341

Lafferty, W. J. & Lovas, F. J. 1978, J. Phys. Chem. Ref. Data, 7, 441

Lilley, A. E. & Palmer, P. 1968, ApJS, 16, 143

Liu, S., Mehringer, D. M., & Snyder, L. E. 2001, ApJ, 552, 654

Lovas, F. J. & Krupenie, P. H. 1974, J. Phys. Chem. Ref. Data, 3, 259

Lovas, F. J. & Tiemann, E. 1974, J. Phys. Chem. Ref. Data, 3, 609

Lovas, F. J. 1978, J. Phys. Chem. Ref. Data, 7, 1445

Lovas, F. J. 1982, J. Phys. Chem. Ref. Data, 11, 251

Lovas, F. J. 1985, J. Phys. Chem. Ref. Data, 14, 395

Lovas, F. J. 2004, J. Phys. Chem. Ref. Data, 33, 1

Martín-Pintado, J., Rizzo, J. R., de Vicente, P., Rodríguez-Fernández, N. J., & Fuente, A. 2001, ApJ, 548, L65

Mehringer, D. M., Snyder, L. E., Miao, Y., & Lovas, F. J. 1997, ApJ, 480, L71

Miao, Y. & Snyder, L. E. 1997, ApJ, 480, L67

Müller, H. S. P., Thorwirth, S., Roth, D. A., & Winnewisser, G. 2001, A&A, 370, L49

Murakami, A. 1990, ApJ, 357, 288

Nummelin, A., Bergman, P., Hjalmarson, Å., Friberg, P., Irvine, W. M., Millar, T. J., Ohishi, M., & Saito, S. 1998, ApJS, 117, 427

Nummelin, A., Bergman, P., Hjalmarson, Å., Friberg, P., Irvine, W. M., Millar, T. J., Ohishi, M., & Saito, S. 2000, ApJS, 128, 213

Oesterling, L. C., Albert, S., de Lucia, F. C., Sastry, K. V. L. N., & Herbst, E. 1999, ApJ, 521, 255

Pickett, H. M., Poynter, R. L., Cohen, E. A., Delitsky, M. L., Pearson, J. C., & Muller, H. S. P. 1998, J. Quant. Spectrosc. & Rad. Transfer 60, 883

Reid, M. J., Schneps, M. H., Moran, J. M., Gwinn, C. R., Genzel, R., Downes, D., & Roennaeng, B. 1988, ApJ, 330, 809

Salter, C., Maddalena, R. J. & Garwood, B. 1995, The Unipops Cookbook

Sault, R. J., Teuben, P. J., & Wright, M. C. H. 1995, in Astronomical Data Analysis Software and Systems IV, ASP Conference Series 77, ed. R. A. Shaw, H. E. Payne, & J. J. E. Hayes, 443

Schilke, P., Walmsley, C. M., Henkel, C., & Millar, T. J. 1991, A&A, 247, 487

Shah, R. Y. & Wootten, A. 2001, ApJ, 554, 933

Snyder, L. E. & Buhl, D. 1974, ApJ, 189, L31

Snyder, L. E., Kuan, Y.-J., & Miao, Y. 1994, The Structure and Content of Molecular Clouds: 25 Years of Molecular Radioastronomy, ed. T. L. Wilson & K. J. Johnston (New York:Springer), 187

Snyder, L. E., Kuan, Y.-J., & Pratap, P. 1991, ASP Conf. Ser. 16: Atoms, Ions and Molecules: New Results in Spectral Line Astrophysics, 191

Snyder, L. E., Lovas, F. J., Mehringer, D. M., Miao, N. Y., Kuan, Y., Hollis, J. M., & Jewell, P. R. 2002, ApJ, 578, 245

Snyder, L. E., Schenewerk, M. S., & Hollis, J. M. 1985, ApJ, 298, 360

Sutton, E. C., Jaminet, P. A., Danchi, W. C., & Blake, G. A. 1991, ApJS, 77, 255

Tiemann, E. J. 1974, J. Phys. Chem. Ref. Data, 3, 259

Turner, B. E. 1989, ApJS, 70, 539

Turner, B. E. 1991, ApJS, 76, 617

Willemot, E., Dangoisse, D., Monnanteuil, N., & Bellet, J. 1980, J. Phys. Chem. Ref. Data, 9, 59

Winnewisser, G., Hocking, W. H., & Gerry, M. C. L. 1976, J. Phys. Chem. Ref. Data, 5, 79

Woods, R. C., Saykally, R. J., Anderson, T. G., Dixon, T. A., & Szanto, P. G. 1981, J. Chem. Phys., 75, 4256

Wright, M. C. H. 1996, BIMA Memoranda Ser. 45

Wyrowski, F., Schilke, P., & Walmsley, C. M. 1999, A&A, 341, 882

Xu, L.-H. & Lovas, F. J. 1997, J. Phys. Chem. Ref. Data, 26, 17

Yamamoto, S., Saito, S., Kawaguchi, K., Chikada, Y., Suzuki, H., Kaifu, N., Ishikawa, S., & Ohishi, M. 1990, ApJ, 361, 318

Yamamoto, S., Saito, S., Suzuki, H., Deguchi, S., Kaifu, N., Ishikawa, S., & Ohishi, M. 1990, ApJ, 348, 363

Watson, W. D. & Salpeter, E. E. 1972, ApJ, 174, 321

Fig. 1.— Pointing centers and average beams from this and previous spectral line surveys of the Sgr B2 region. The five cores of Sgr B2 are labeled (North, Main, South, Northwest, and OH). The beams from this survey are in bold face centered on Sgr B2(N). The dashed beams around Sgr B2(N), Sgr B2(M), and Sgr B2(NW) are from Nummelin et al. (1998, 2000). The grey beams around Sgr B2(N) and Sgr B2(M) (2 beams) are from Sutton et al. (1991). The beams centered on Sgr B2(OH) are from Turner (1989, 1991) and Cummins, Thaddeus, & Linke (1986).

Fig. 2.— Frequency coverage of the line survey. 12 meter telescope coverage is in black. BIMA Array coverage is in grey. Some frequencies are covered by the BIMA Array and not the 12 meter telescope due to the dual sidebands of the BIMA Array receiver and correlator systems. Only frequencies which have been observed by both instruments are presented in this paper.

Fig. 3.— The top spectra are from the BIMA Array. The vertical dashed lines denote where two spectral windows meet. The bars next to the window edges denote the rms noise level of each window. The bottom spectra are from the NRAO 12 meter and match the BIMA Array frequency range. The 12 meter telescope intensity scale was converted from T_R^* to Jy beam^{-1} using 30.5, 30.6, 30.8, 31.6, 31.8, 32.0 Jy K^{-1} as conversion factors for the 86.2, 86.8, 90.025, 106.58, 108.5 and 110.2 GHz bands, respectively. Detected transitions of known lines are noted, as are lines from unknown transitions (denoted as U).

Fig. 4.— Maps from the BIMA Array toward Sgr B2(N-LMH) of 4 representative molecular species. In each map the continuum is mapped in grey scale with the transition, averaged over the FWHM of the line, mapped in contours. The central continuum peak is Sgr B2(N-LMH) and the lower continuum peak is Sgr B2(M). The BIMA Array and 12 meter telescope spectra of each mapped transition is below their respective maps. The vertical axis is intensity in Jy beam^{-1} and the horizontal axis is frequency in GHz. The synthesized beam is given in the lower left corner of each map. The numbers on the grey scale wedge are in Jy beam^{-1}. (a) Map of the 106.541 GHz, $5_{2,3}$-$4_{2,2}$ transition of NH_2CHO (formamide). The contours are 3, 6, 9, 12, 15, 18, and 21σ. (b) The 90.117 GHz, $4_{1,4}$-$3_{0,3}$ transition of C_2H_5OH (ethanol, EtOH). The contours are -2, -1, 1, 3, and 4.5σ. (c) Map of the 86.093 GHz, 2_2-1_1 transition of SO. The contours are -6, -3, 3, 6, 9, 12, 15, 18, 21, and 24σ. (d) Map of the 86.340 GHz, $1_{0,1}$-$0_{0,0}$ transition of $H^{13}CN$. The contours are -14, -12, -9, -6, -3, and 3σ.

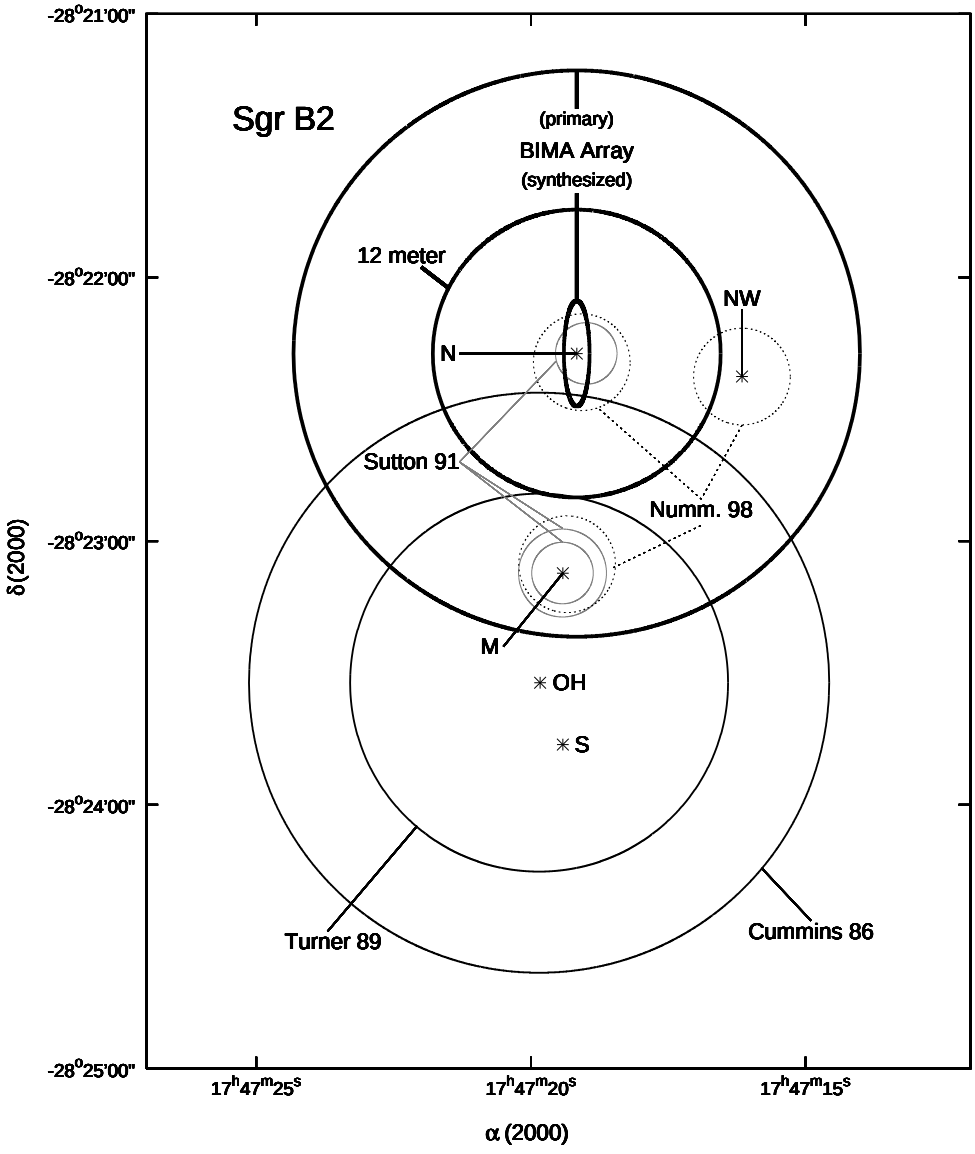
Sgr B2
(primary)
BIMA Array
(synthesized)
12 meter
NW
N
Sutton 91
Numm. 98
M
OH
S
Turner 89
Cummins 86
-28°21'00"
-28°22'00"
-28°23'00"
-28°24'00"
-28°25'00"
δ(2000)
17h47m25s
17h47m20s
17h47m15s
α(2000)

Figure 1

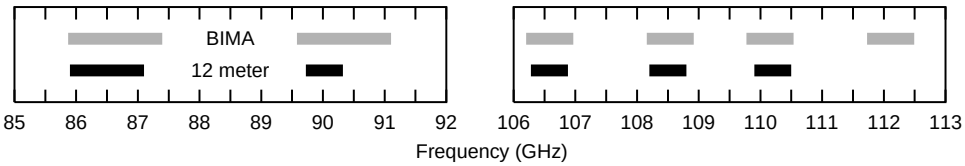
BIMA
12 meter
85
86
87
88
89
90
91
92
106
107
108
109
110
111
112
113
Frequency (GHz)

Figure 2

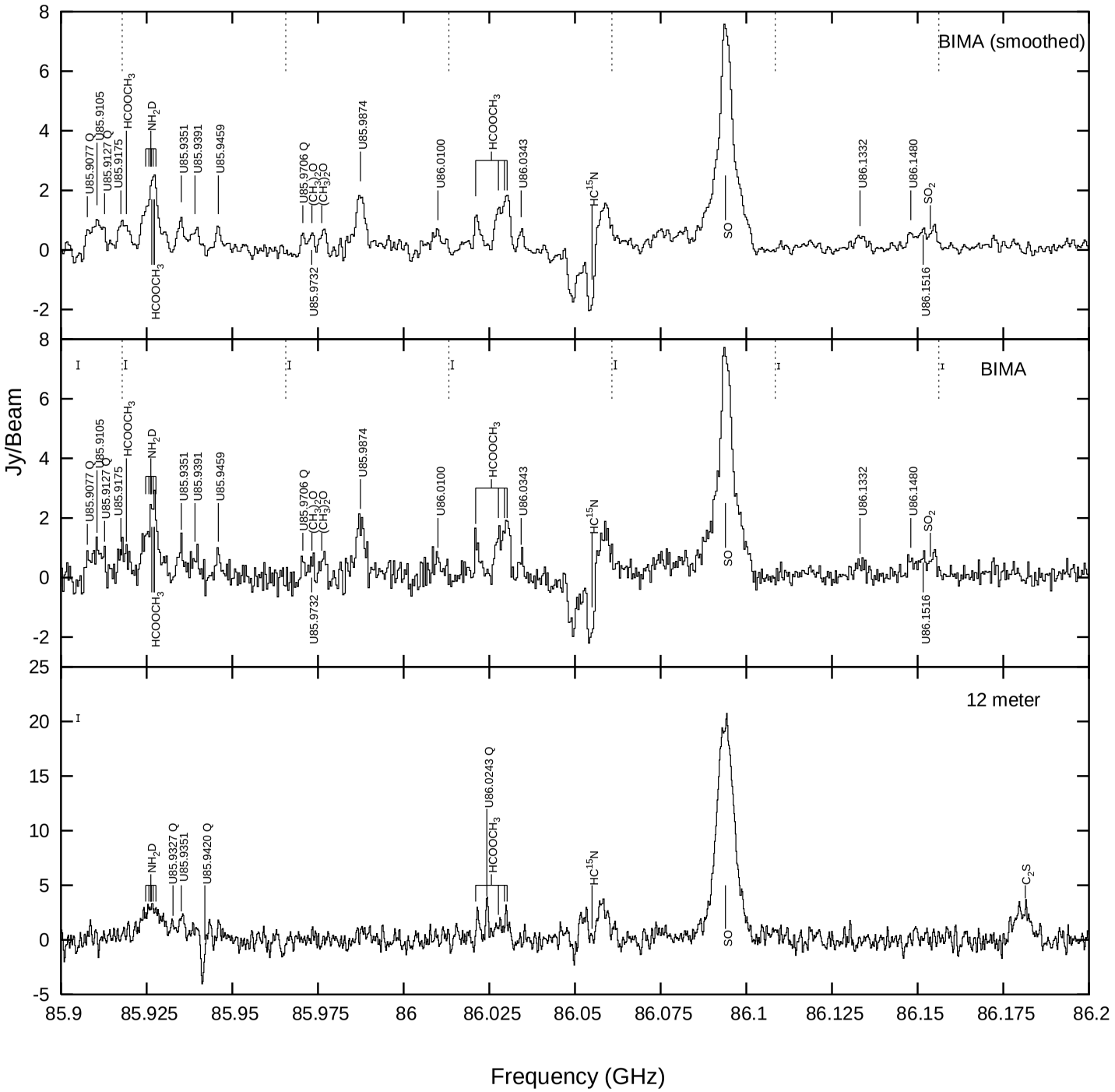
BIMA (smoothed)
BIMA
12 meter
Jy/Beam
Frequency (GHz)
U85.9077 Q
U85.9105
U85.9127 Q
U85.9175
HCOOCH3
NH2D
HCOOCH3
U85.9351
U85.9391
U85.9459
U85.9706 Q
(CH3)2O
(CH3)2O
U85.9732
U85.9874
U86.0100
HCOOCH3
U86.0343
HC15N
SO
U86.1332
U86.1480
SO2
U86.1516
U86.0243 Q
NH2D
U85.9327 Q
U85.9351
U85.9420 Q
C2S

Figure 3a

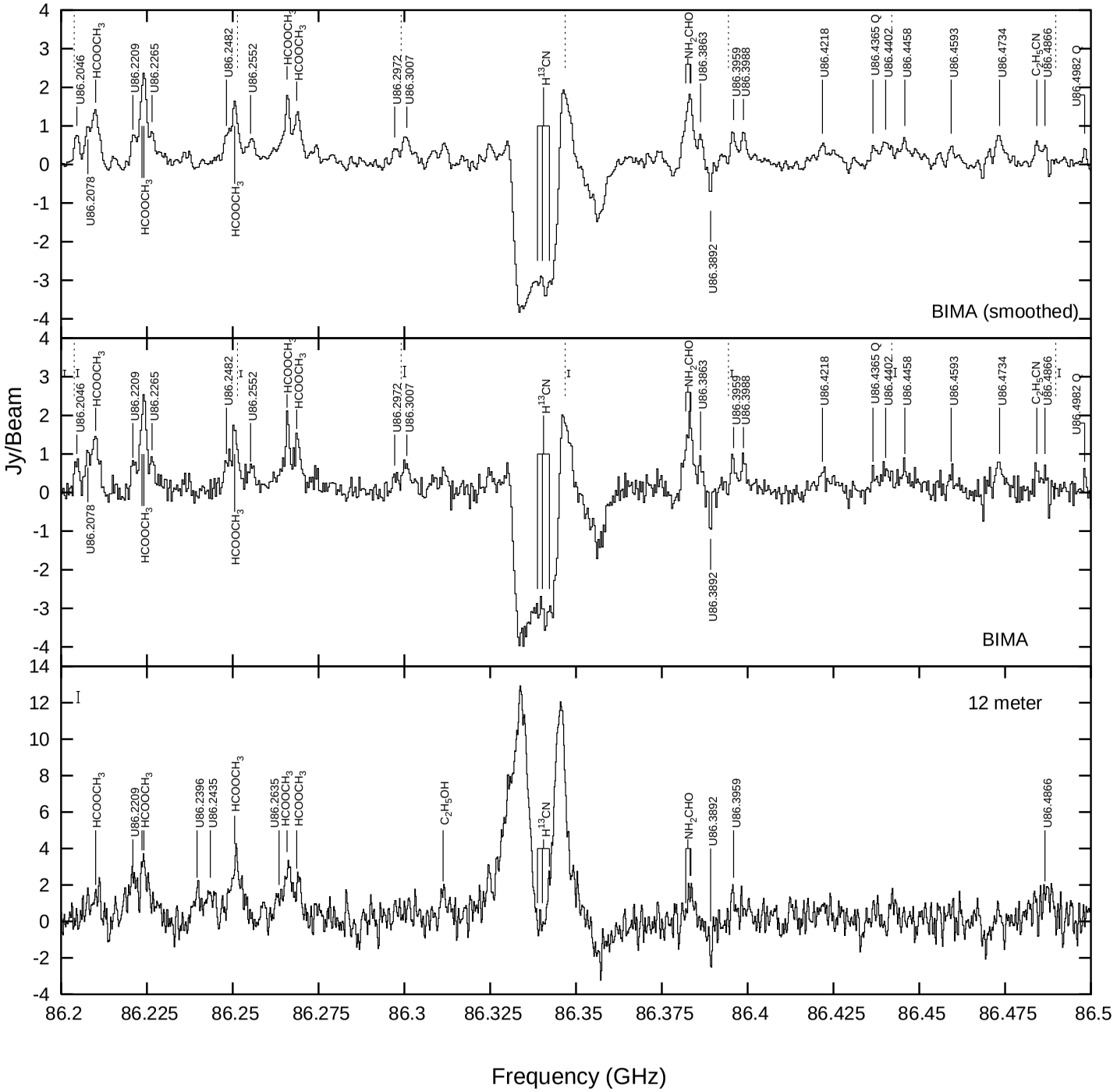
BIMA (smoothed)
BIMA
12 meter
Jy/Beam
Frequency (GHz)
U86.2046
HCOOCH3
U86.2078
U86.2209
HCOOCH3
U86.2265
U86.2482
HCOOCH3
U86.2552
HCOOCH3
HCOOCH3
U86.2972
U86.3007
H13CN
NH2CHO
U86.3863
U86.3892
U86.3959
U86.3988
U86.4218
U86.4365 Q
U86.4402
U86.4458
U86.4593
U86.4734
C2H5CN
U86.4866
U86.4982 Q
U86.2396
U86.2435
U86.2635
C2H5OH

Figure 3b

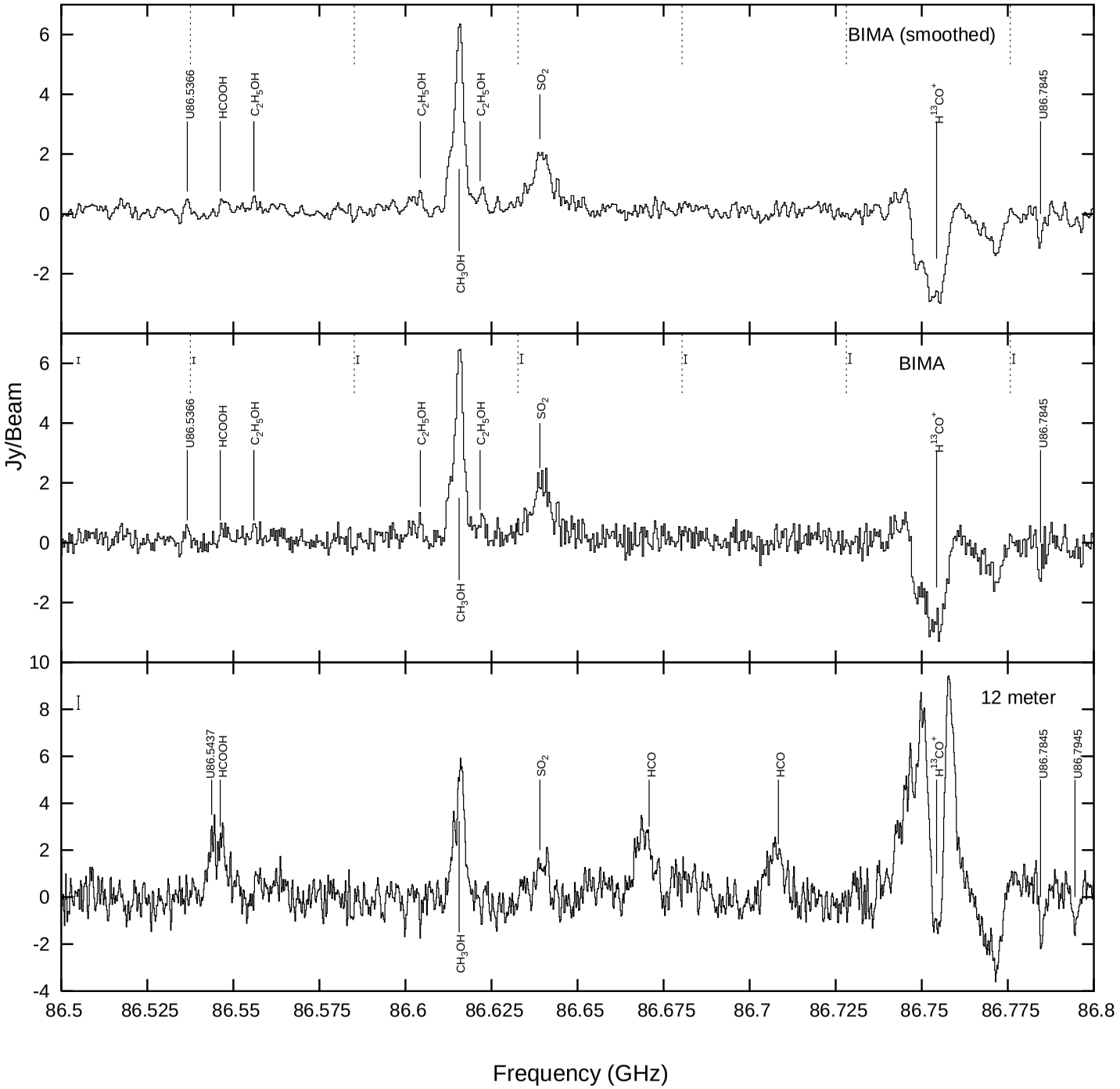
BIMA (smoothed)
BIMA
12 meter
Jy/Beam
Frequency (GHz)
U86.5366
HCOOH
C2H5OH
CH3OH
SO2
H13CO+
U86.7845
U86.5437
U86.7945
HCO

Figure 3c

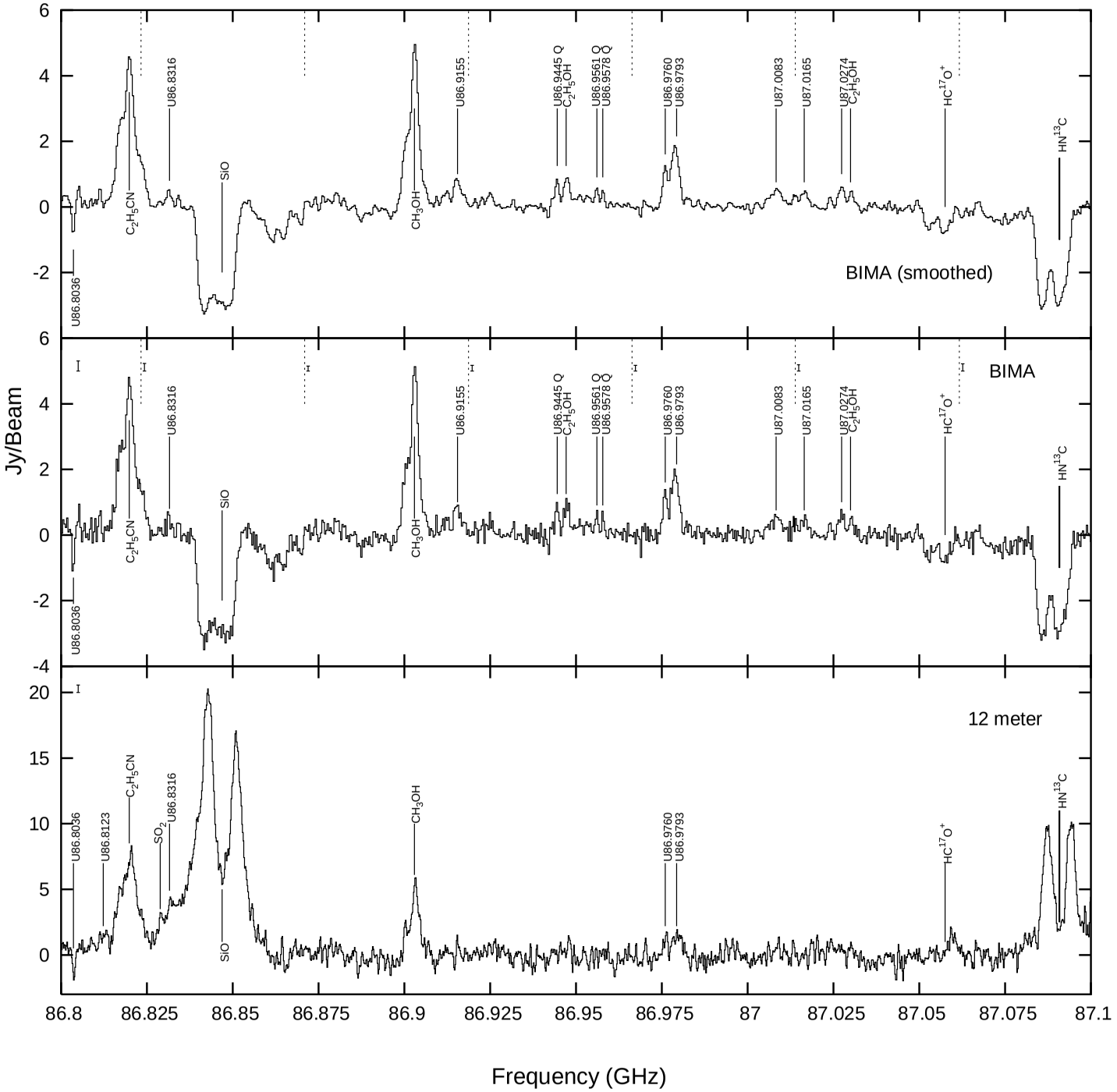
BIMA (smoothed)
BIMA
12 meter
Jy/Beam
Frequency (GHz)
U86.8036
C2H5CN
U86.8316
SiO
CH3OH
U86.9155
U86.9445 Q
C2H5OH
U86.9561 Q
U86.9578 Q
U86.9760
U86.9793
U87.0083
U87.0165
U87.0274
C2H5OH
HC17O+
HN13C
U86.8123
SO2

Figure 3d

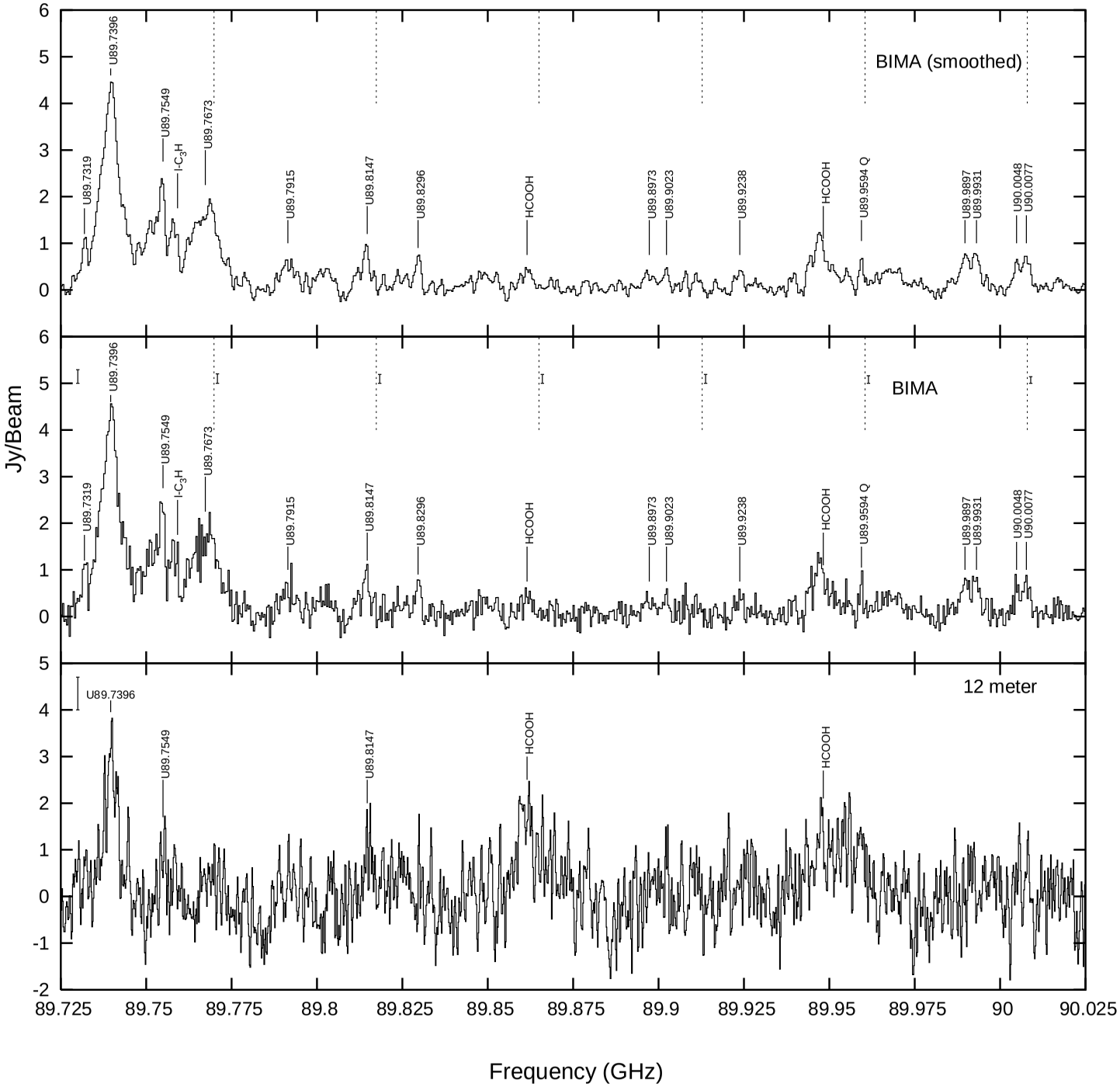
BIMA (smoothed)
BIMA
12 meter
Jy/Beam
Frequency (GHz)
U89.7319
U89.7396
U89.7549
l-C3H
U89.7673
U89.7915
U89.8147
U89.8296
HCOOH
U89.8973
U89.9023
U89.9238
HCOOH
U89.9594 Q
U89.9897
U89.9931
U90.0048
U90.0077

Figure 3e

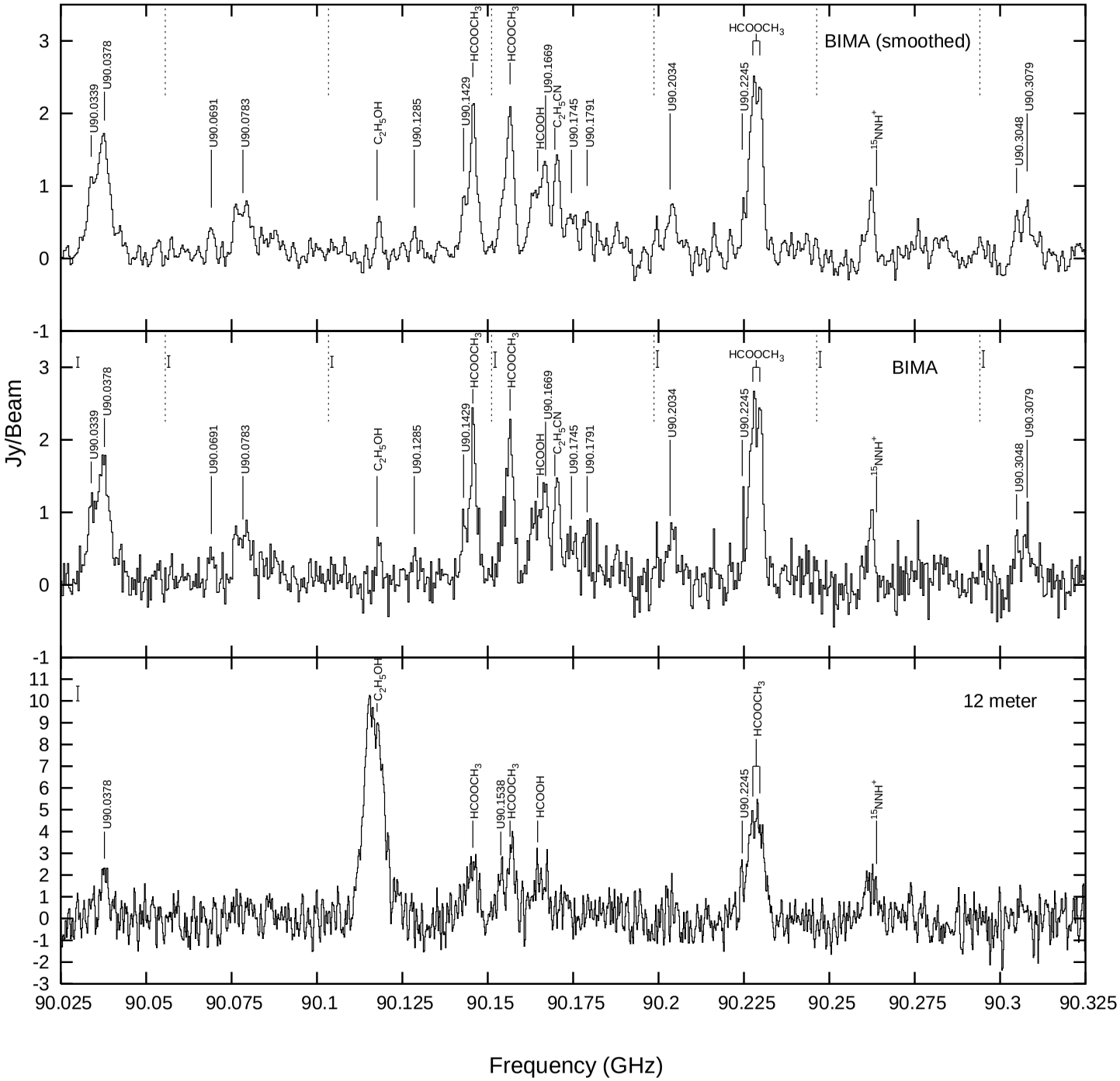
BIMA (smoothed)
BIMA
12 meter
Jy/Beam
Frequency (GHz)
U90.0339
U90.0378
U90.0691
U90.0783
C2H5OH
U90.1285
U90.1429
HCOOCH3
HCOOH
U90.1669
C2H5CN
U90.1745
U90.1791
U90.2034
U90.2245
15NNH+
U90.3048
U90.3079
U90.1538

Figure 3f

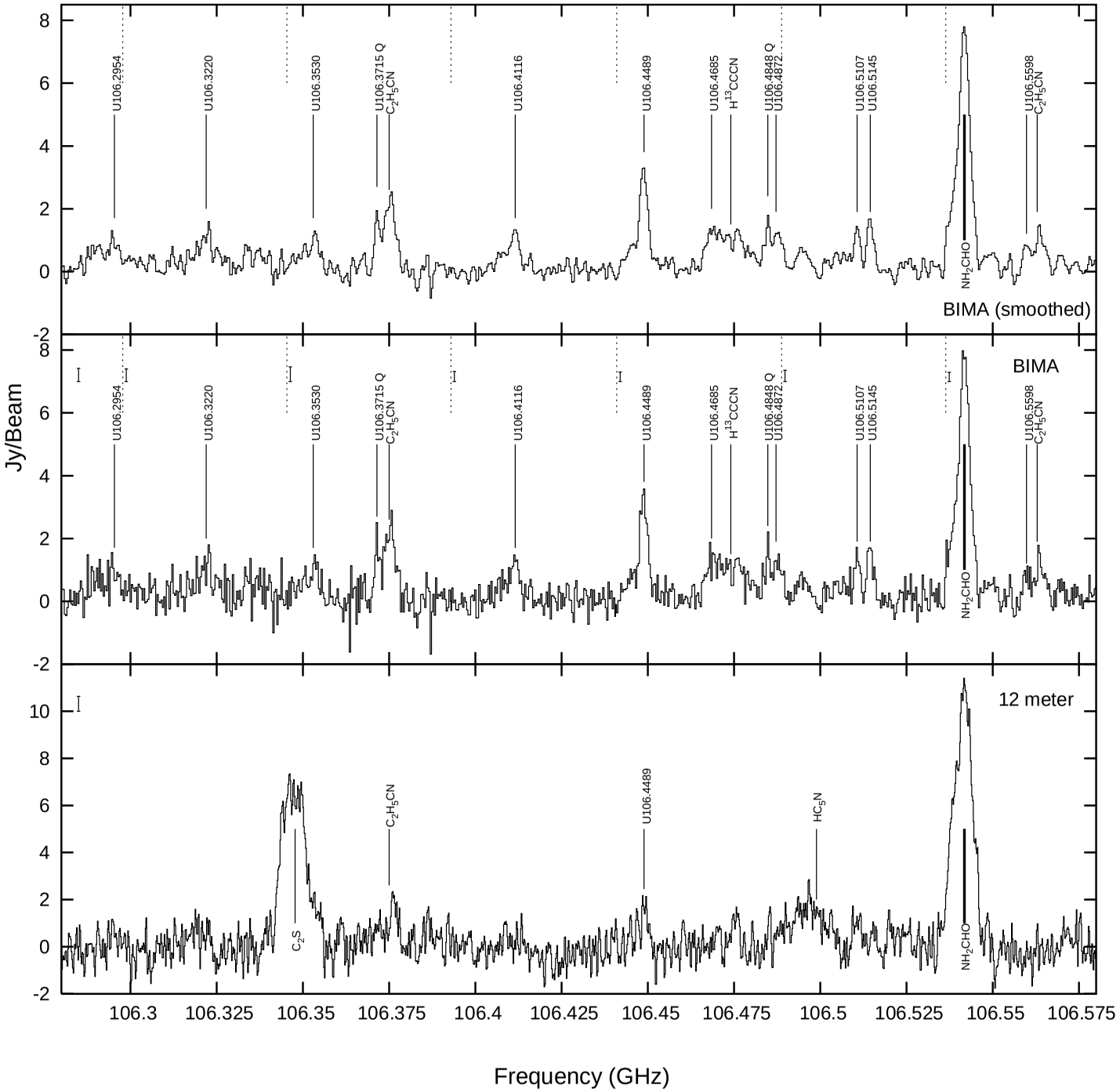
BIMA (smoothed)
BIMA
12 meter
Jy/Beam
Frequency (GHz)
U106.2954
U106.3220
U106.3530
U106.3715 Q
C2H5CN
U106.4116
U106.4489
U106.4685
H13CCN
U106.4848 Q
U106.4872
U106.5107
U106.5145
U106.5598
NH2CHO
C2S
HC5N

Figure 3g

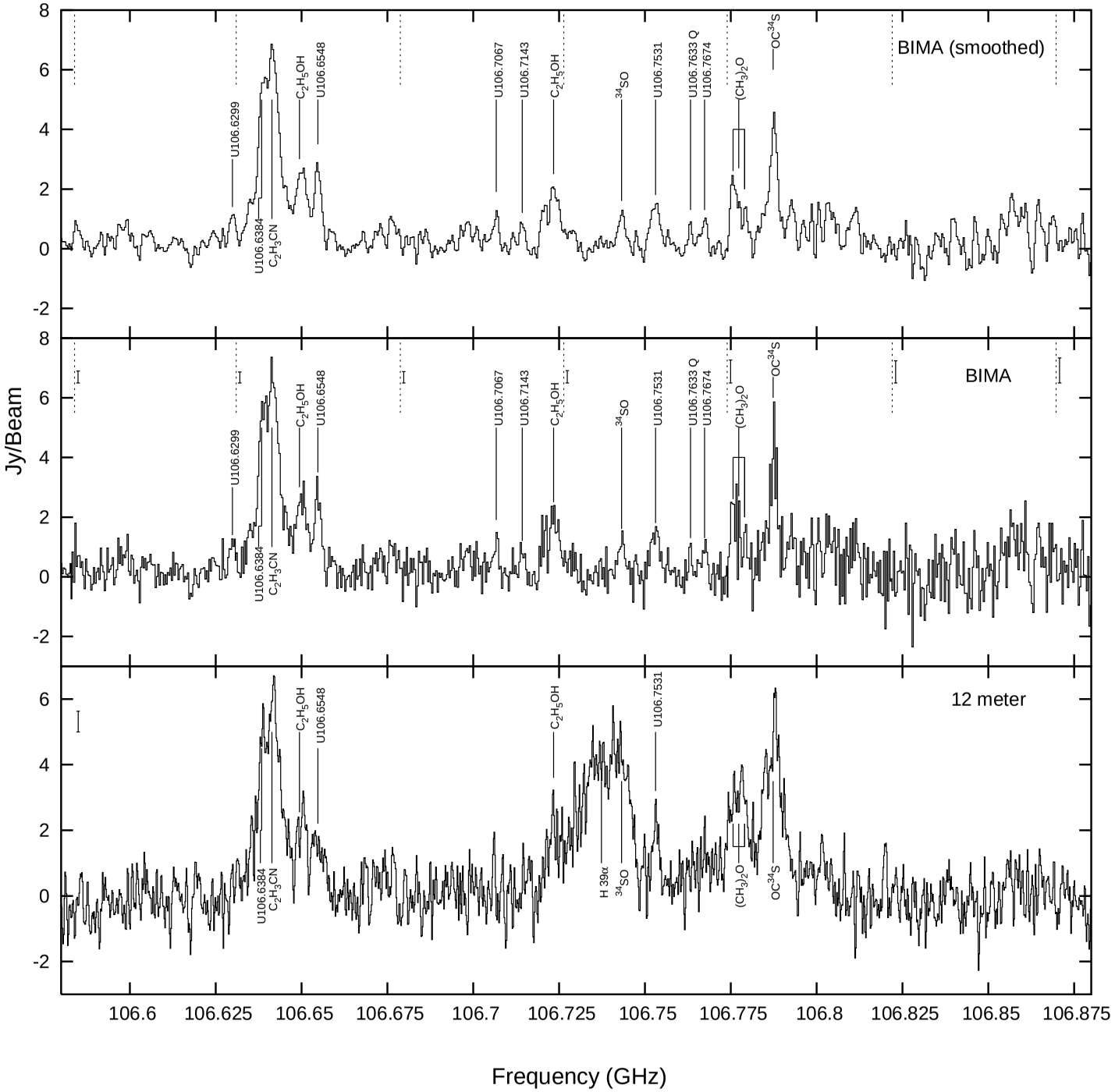
BIMA (smoothed)
BIMA
12 meter
Jy/Beam
Frequency (GHz)
U106.6299
U106.6384
C2H3CN
C2H5OH
U106.6548
U106.7067
U106.7143
C2H3OH
34SO
U106.7531
U106.7633 Q
U106.7674
(CH3)2O
OC34S
H 39α

Figure 3h

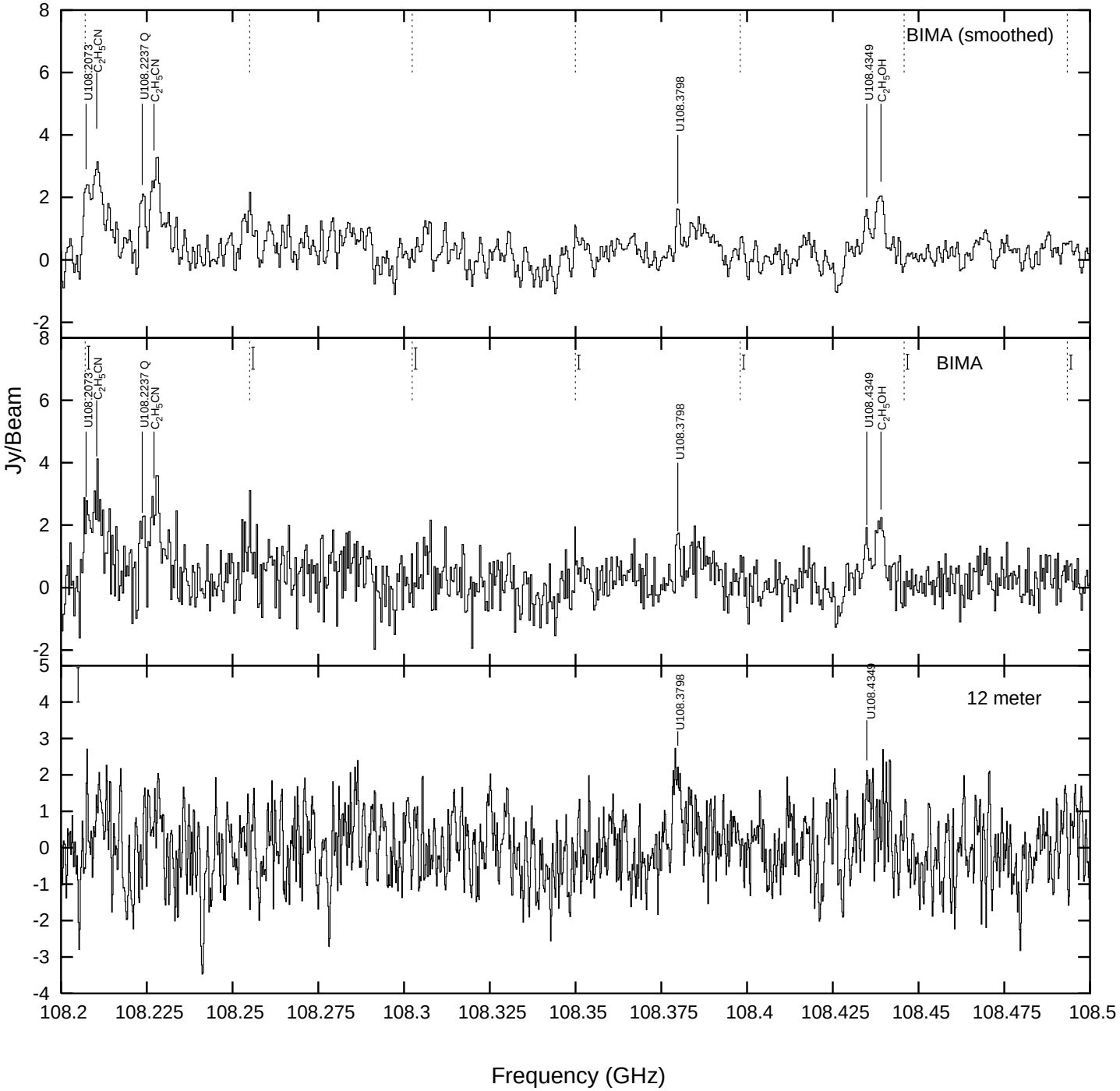
BIMA (smoothed)
BIMA
12 meter
U108.2073
C2H5CN
U108.2237 Q
C2H5CN
U108.3798
U108.4349
C2H5OH
Jy/Beam
Frequency (GHz)

Figure 3i

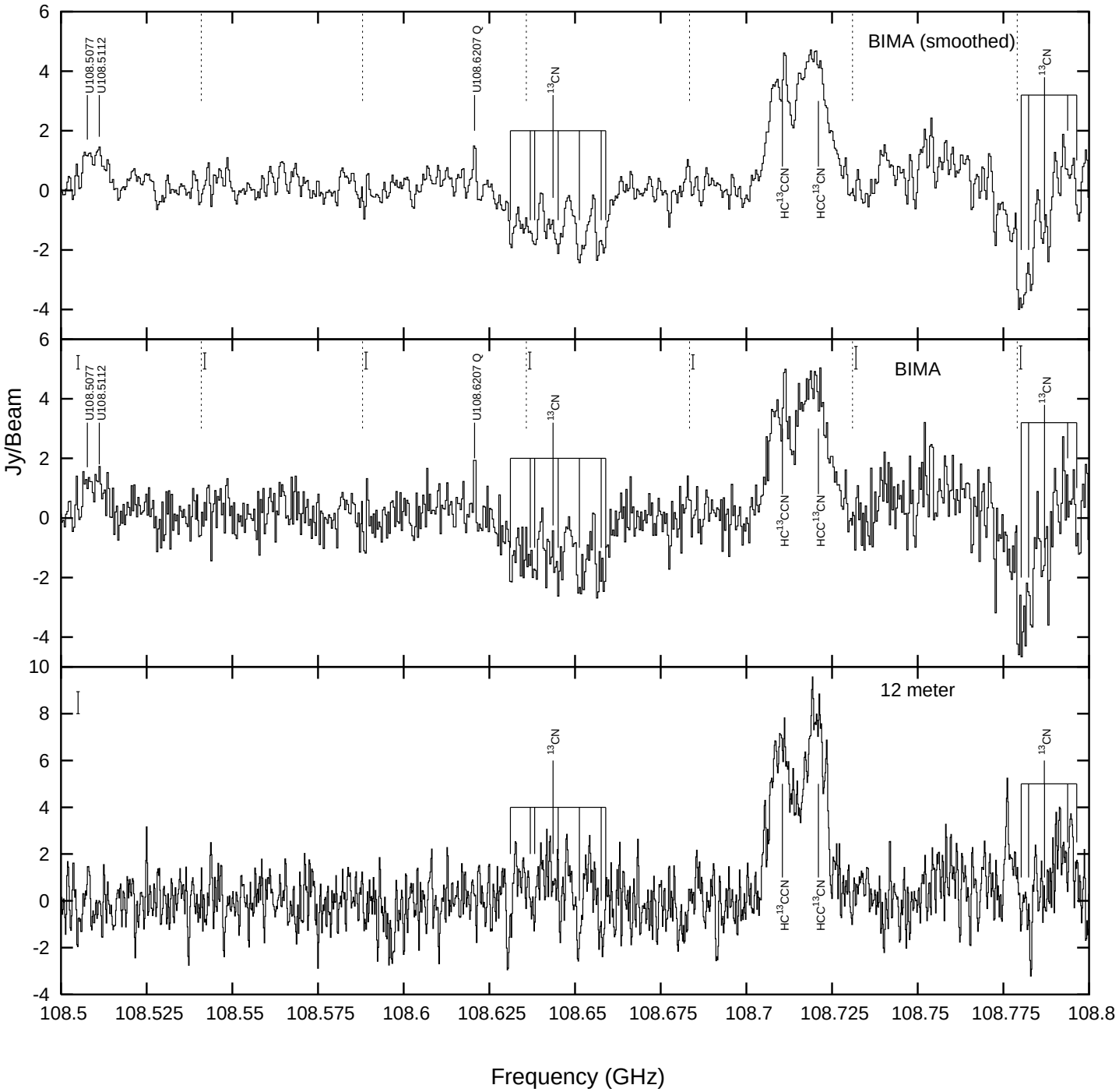
BIMA (smoothed)
BIMA
12 meter
U108.5077
U108.5112
U108.6207 Q
13CN
HC13CCN
HCC13CN
Jy/Beam
Frequency (GHz)

Figure 3j

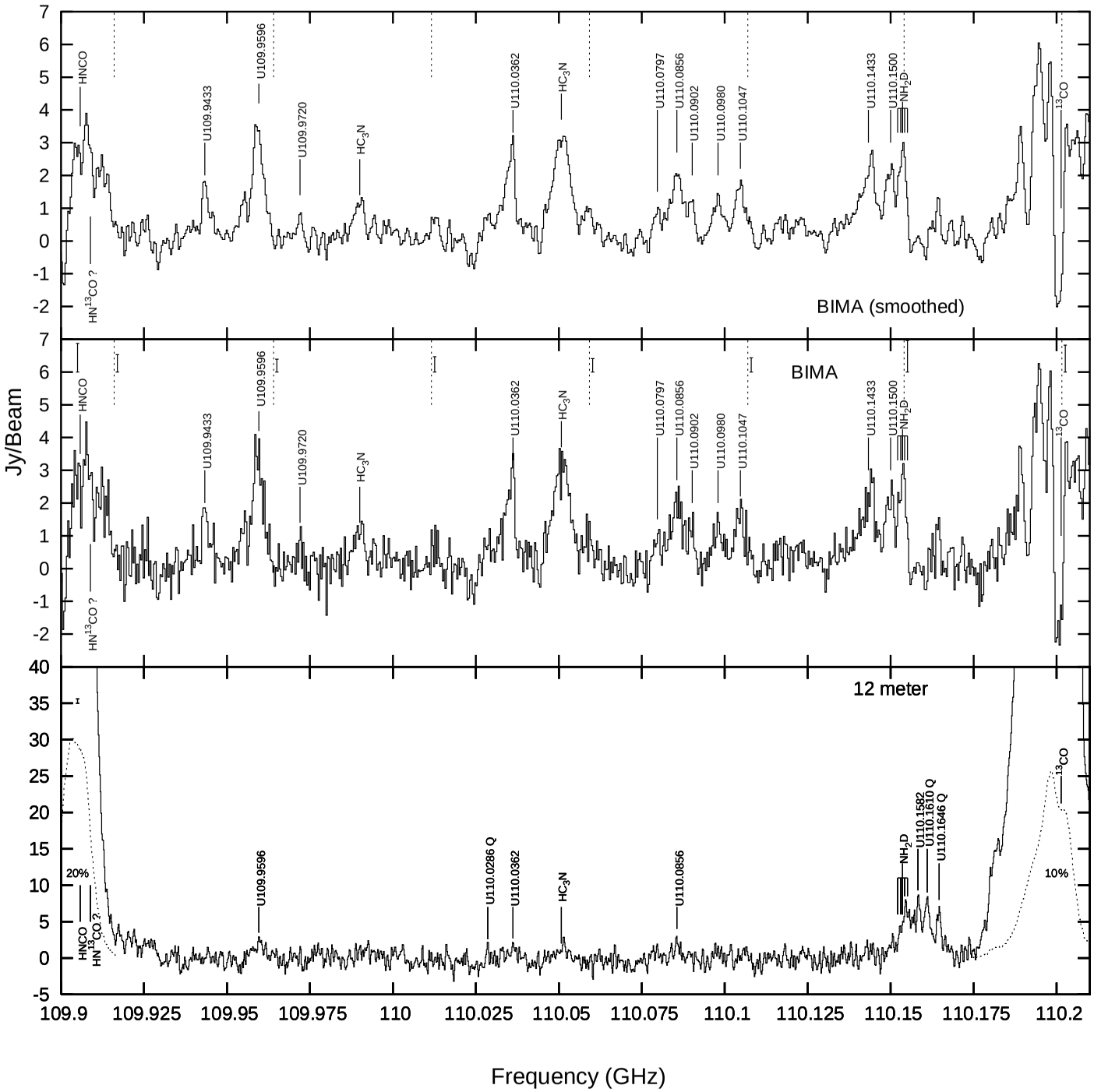
BIMA (smoothed)
BIMA
12 meter
Jy/Beam
Frequency (GHz)
HNCO
HN13CO ?
U109.9433
U109.9596
U109.9720
HC3N
U110.0362
U110.0797
U110.0856
U110.0902
U110.0980
U110.1047
U110.1433
U110.1500
NH2D
13CO
U110.0286 Q
U110.1582
U110.1610 Q
U110.1646 Q
20%
10%

Figure 3k

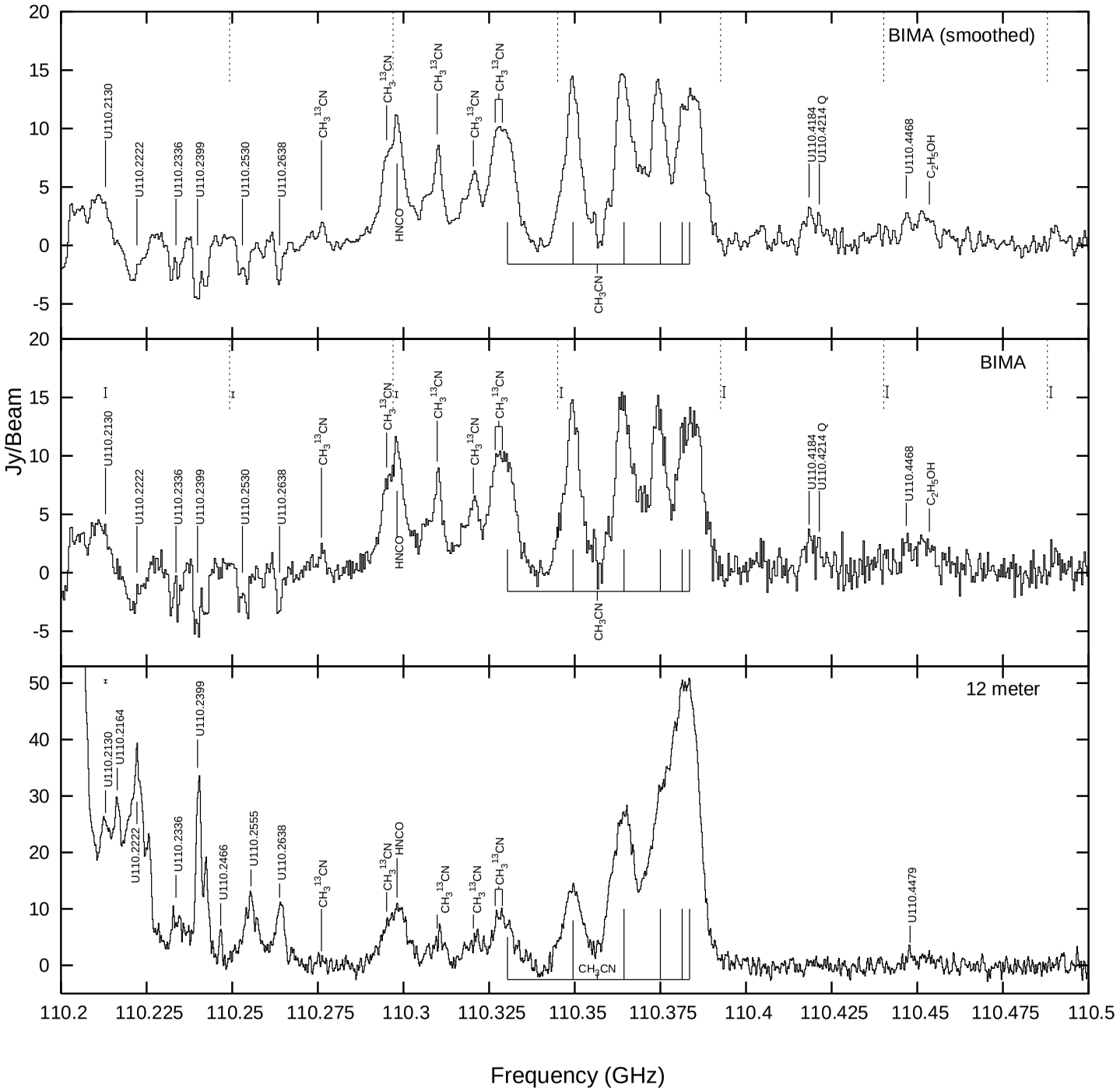
BIMA (smoothed)
BIMA
12 meter
Jy/Beam
Frequency (GHz)
U110.2130
U110.2222
U110.2336
U110.2399
U110.2530
U110.2638
CH3 13CN
HNCO
U110.4184
U110.4214 Q
U110.4468
C2H5OH
U110.2164
U110.2466
U110.2555
U110.4479
CH3CN

Figure 3l

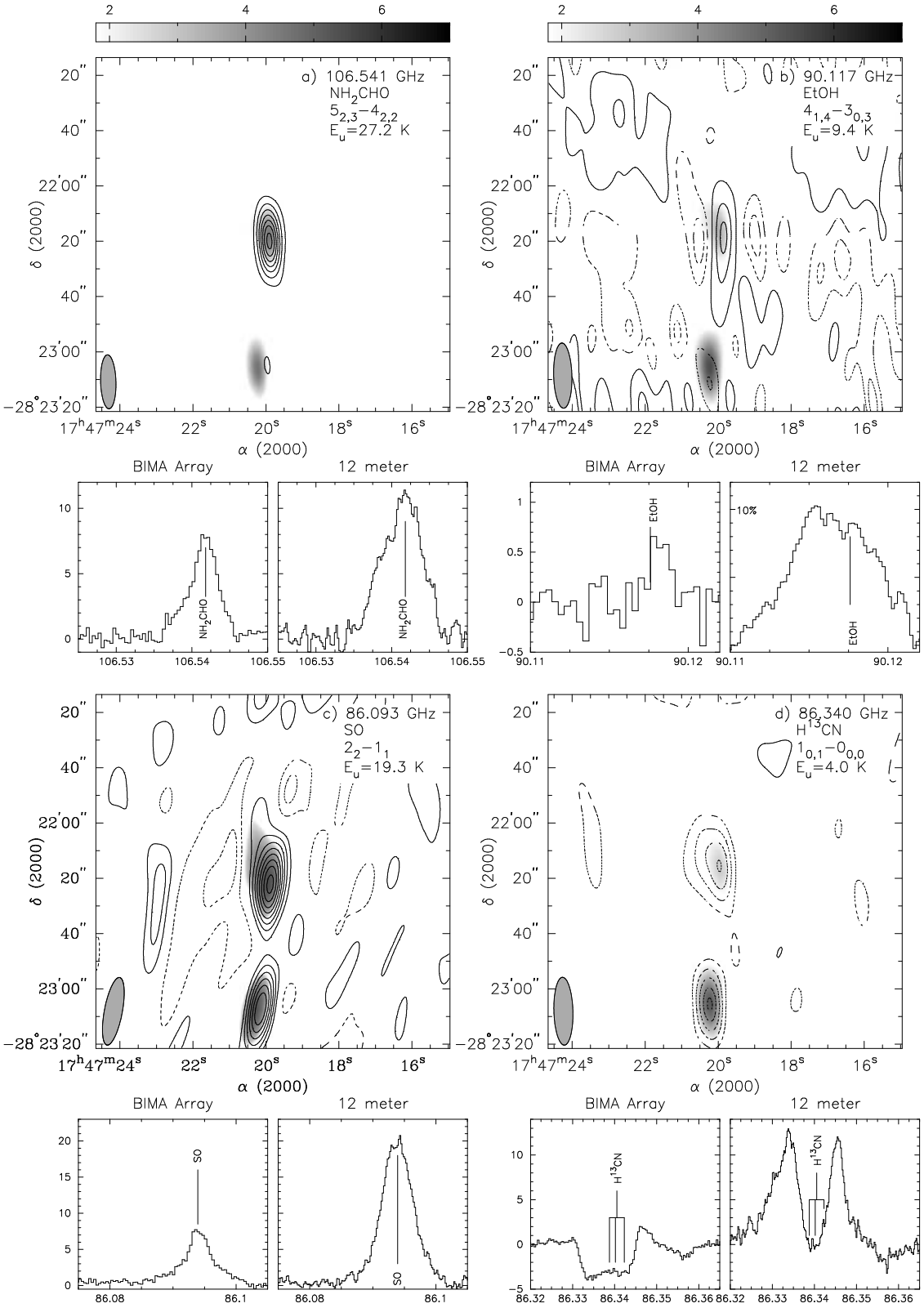
a) 106.541 GHz
NH2CHO
5 2,3 − 4 2,2
Eu=27.2 K
b) 90.117 GHz
EtOH
4 1,4 − 3 0,3
Eu=9.4 K
c) 86.093 GHz
SO
2 2 − 1 1
Eu=19.3 K
d) 86.340 GHz
H13CN
1 0,1 − 0 0,0
Eu=4.0 K
δ (2000)
α (2000)
BIMA Array
12 meter
NH2CHO
EtOH
SO
H13CN
10%

Figure 4

Table 1. Coordinates of Sources

Source	α(J2000)	δ(J2000)
Sgr B2(N-LMH)[a]	$17^h47^m20^s.0$	$-28^\circ22'17''.3$
Sgr B2(M)[b]	$17^h47^m20^s.3$	$-28^\circ23'07''.3$
Sgr B2(OH)[b]	$17^h47^m20^s.8$	$-28^\circ23'32''.2$
Sgr B2(S)[b]	$17^h47^m20^s.3$	$-28^\circ23'46''.3$
Sgr B2(NW)[c]	$17^h47^m16^s.4$	$-28^\circ22'22''.5$

[a]Taken from Miao & Snyder (1997)

[b]Taken from Sutton et al. (1991)

[c]Taken from Nummelin et al. (1998)

Table 2. Beam Sizes[a] and RMS Noise Levels of Observations

	BIMA Array		12 meter telescope	
Frequency (GHz.)	Beam[b] ($''\times''$)	RMS[b] (Jy/beam)	Beam ($''$)	RMS (Jy/beam)
86.200	27.2×6.6	0.216	74	0.613
86.800	32.2×6.5	0.231	73	0.569
90.025	25.2×6.3	0.197	71	0.700
106.580	23.2×5.2	0.462	60	0.628
108.500	21.0×5.3	0.586	59	0.941
110.200	23.2×5.1	0.679	57	0.598

[a]Synthesized beam for BIMA Array observations and main diffraction beamwidth (FWHM) for 12 meter telescope observations.

[b]Average of all scans.

Table 3. Summary of Molecules Detected by the BIMA Array and NRAO 12 Meter Radio Telescope

	Detected Transitions		
Species	BIMA Array	12 meter telescope	Reference
l-C_3H[a]	1	0	1,2,3
C_2H_3CN	1	1	4
C_2H_5CN	7	2	5
C_2H_5OH	11	4	5,6
C_2S	0	2	7,8
CH_3CN	6	6	9
$CH_3^{13}CN$	6	6	9
$(CH_3)_2O$	6	4	10
CH_3OH	2	2	11
^{13}CN[a]	4	4	12
^{13}CO	1	1	13
$H^{39}\alpha$	0	1	14
HC_5N	0	1	3,15
HC_3N	2	1	15,16,17
$H^{13}CCCN$	1	0	15,17
$HC^{13}CCN$	1	1	16
$HCC^{13}CN$	1	1	16
$H^{13}CN$[a]	1	1	18
$HC^{15}N$	1	1	18
HCO[a]	0	1	3,19
$H^{13}CO^+$	1	1	20
$HC^{17}O^+$	1	1	21
$HCOOCH_3$	18	14	22
HCOOH	4	4	23
$HN^{13}C$[a]	1	1	3,24
HNCO	2	2	3,25
$HN^{13}CO$	1	1	26
NH_2CHO[a]	2	2	26
NH_2D[a]	2	2	3,27,28
$^{15}NNH^+$	1	1	3,15
$OC^{34}S$	1	1	3,18
SiO	1	1	29
SO	1	1	30
^{34}SO	1	1	30
SO_2	2	2	31
U	108	41	...
Totals	199	116	

[a]Number of detected lines does not include hyperfine components.

References. — (1) Gottlieb et al. (1986) (2) Yamamoto et al. (1990b); (3) Pickett et al. (1998); (4) Gerry, Yamada, & Winnewisser (1979); (5) Lovas (1982); (6) J. C. Pearson, private communication; (7) Yamamoto et al. (1990a); (8) Murakami (1990); (9) Boucher et al. (1980); (10) Groner et al. (1998); (11) Xu & Lovas (1997); (12) Bogey, Demuynck, & Destombles (1984); (13) Lovas & Tiemann (1974); (14) Lilley & Palmer (1968); (15) Lovas (2004); (16) Lafferty & Lovas (1978); (17) Wyrowski, Schilke, & Walmsley (1999); (18) Lovas (1978); (19) Snyder, Schenewerk, & Hollis (1985); (20) Woods et al. (1981); (21) Guelin, Cernicharo, & Linke (1982); (22) Oesterling et al. (1999); (23) Willemot et al. (1980); (24) Frerking, Wilson, & Langer (1979); (25) Winnewisser, Hocking, & Gerry (1976); (26) Johnson, Lovas, & Kirchhoff (1972); (27) Bester et al. (1983); (28) Shah & Wootten (2001); (29) Lovas & Krupenie (1974); (30) Tiemann (1974); (31) Lovas (1985)

Table 4. Detected Transitions

Rest Frequency (MHz)[a]	Transition[b]	BIMA Array I_0 (Jy bm^{-1})	BIMA Array Δv (km s^{-1})	12 meter telescope I_0 (Jy bm^{-1})	12 meter telescope Δv (km s^{-1})	E_u (K)	$\langle S_{i,j}\mu^2 \rangle$ (D^2)
		l-C_3H ($\nu_4^2\Sigma^\mu$)					
89,759.3280 (480)[c]	$N_J = 4\frac{7}{2} - 3\frac{5}{2}$, $F = 4-3$	1.0(8)	7.0(56)	< 0.7	···	49.9	18.45
89,759.8490 (480)[c]	$F = 3-2$	···	···	< 0.7	···	49.9	13.74
		C_2H_3CN (VyCN)					
106,641.3940 (170)	$11_{1,10} - 10_{1,9}$	6.7(4)	11.7(38)	6.1(4)	10.7(18)	32.9	147.71
		C_2H_5CN (EtCN)					
86,484.2300 (400)[d]	$29_{3,27} - 28_{4,24}$	0.5(2)	5.9(38)	< 0.6	···	197.1	6.20
86,819.8510 (130)[e]	$10_{1,10} - 9_{1,9}$	4.6(2)	11.4(10)	7.5(2)	13.8(14)	24.1	146.68
90,169.6330 (260)[d]	$20_{2,18} - 19_{3,17}$	1.5(2)	6.6(18)	< 0.7	···	96.4	6.09
106,375.0030 (200)	$15_{3,12} - 15_{2,13}$	2.4(4)	10.9(26)	2.0(4)	7.6(28)	61.7	13.24
106,562.9160 (320)[d]	$27_{3,24} - 26_{4,23}$	1.3(4)	9.6(28)	< 0.6	···	174.1	7.23
108,210.3860 (170)[d]	$11_{1,11} - 10_{0,10}$	2.7(6)	13.8(70)	< 0.9	···	28.6	11.01
108,227.0930 (200)[d]	$14_{3,11} - 14_{2,12}$	2.6(8)	13.0(52)	< 0.9	···	55.2	12.07
		C_2H_5OH[f](EtOH)					
86,311.2673 (32)[d]	$5^+_{2,4} - 4^+_{2,3}$	< 0.3	···	1.8(2)	6.0(10)	73.7	5.03
86,555.9124 (28)[c,d]	$5^+_{4,2} - 4^+_{4,1}$	0.7(4)	4.4(26)	< 0.6	···	88.3	4.20
86,556.0115 (28)[c,d]	$5^+_{4,1} - 4^+_{4,0}$	···	···	···	···	88.3	4.20
86,604.2917 (28)[d]	$5^+_{3,3} - 4^+_{3,2}$	0.9(2)	4.3(16)	< 0.6	···	79.8	4.07
86,621.7341 (28)[d]	$5^+_{3,2} - 4^+_{3,1}$	0.9(2)	7.5(24)	< 0.6	···	79.8	4.07
86,947.1200 (270)[d]	$15_{2,13} - 15_{1,14}$	0.9(4)	7.2(30)	< 0.6	···	108.1	22.56
87,029.9919 (30)[d]	$5^+_{2,3} - 4^+_{2,2}$	0.6(2)	4.2(22)	< 0.6	···	73.8	5.02
90,117.6000 (90)	$4_{1,4} - 3_{0,3}$	0.6(2)	4.7(22)	9.9(4)	21.5(10)	9.4	5.35
106,649.4400 (310)[d]	$13_{1,12} - 13_{0,13}$	2.7(4)	11.4(32)	2.5(4)	7.8(26)	79.4	10.14
106,723.4100 (180)	$9_{2,8} - 9_{1,9}$	1.9(4)	11.3(44)	1.7(4)	10.4(34)	42.7	7.66
108,439.0700 (800)[d]	$13_{3,10} - 13_{2,11}$	2.2(2)	7.8(12)	< 0.6	···	88.2	18.19
110,453.5300 (3990)[d]	$21_{3,18} - 21_{2,19}$	2.7(6)	15.4(48)	< 0.6	···	208.7	33.93
		C_2S					
86,181.4130 (100)	$J_N = 6_7 - 5_6$	< 0.2	···	2.8(4)	18.7(24)	23.3	41.03
106,347.7420 (100)	$J_N = 9_8 - 8_7$	< 0.5	···	7.1(4)	22.4(12)	24.5	63.01
		CH_3CN					
110,330.3470 (23)[g]	$J_K = 6_5 - 5_5$	6.0(12)	19.8(10)	3.1(10)	20.9(6)	196.1	28.07
110,349.4730 (16)	$J_K = 6_4 - 5_4$	13.1(10)	15.8(14)	12.5(12)	20.9(6)	132.2	51.03
110,364.3570 (11)	$J_K = 6_3 - 5_3$	14.1(10)	17.7(16)	26.8(12)	20.9(6)	82.5	68.90
110,374.9920 (9)	$J_K = 6_2 - 5_2$	12.6(10)	18.0(22)	27.1(18)	20.9(6)	47.0	81.66
110,381.3760 (10)	$J_K = 6_1 - 5_1$	10.7(18)	12.0(16)	16.1(42)	20.9(6)	25.7	89.31
110,383.5040 (10)	$J_K = 6_0 - 5_0$	10.9(18)	12.0(16)	36.5(42)	20.9(6)	18.5	91.87
		$CH_3^{13}CN$					
110,276.0470 (460)[d]	$J_K = 6_5 - 5_5$	1.2(4)	17.2(4)	0.6(4)	15.4(8)	197.5	28.07
110,295.0700 (340)[d]	$J_K = 6_4 - 5_4$	3.2(18)	17.2(4)	5.3(4)	15.4(8)	133.1	51.03
110,309.8670 (290)	$J_K = 6_3 - 5_3$	6.8(4)	17.2(4)	4.5(4)	15.4(8)	83.0	68.90
110,320.4350 (290)[d]	$J_K = 6_2 - 5_2$	5.4(4)	17.2(4)	4.4(4)	15.4(8)	47.2	81.66
110,326.7770 (300)[g]	$J_K = 6_1 - 5_1$	1.6(12)	17.2(4)	1.5(8)	15.4(8)	25.7	89.31
110,328.8900 (310)[g]	$J_K = 6_0 - 5_0$	4.3(22)	17.2(4)	4.9(16)	15.4(8)	18.5	91.87
		$(CH_3)_2O$					
85,973.2490 (80)	$13_{2,12} - 12_{3,9}$AA	0.3(2)	5.6(30)	< 0.6	···	88.0	2.81
85,976.1310 (80)	$13_{2,12} - 12_{3,9}$EE	0.8(4)	5.6(30)	< 0.6	···	88.0	2.81
106,775.6790 (80)	$9_{1,8} - 8_{2,7}$AA	0.9[h]	7.0	1.1(2)	15.7(26)	43.4	3.66
106,777.3710 (60)	$9_{1,8} - 8_{2,7}$EE	1.4[h]	7.0	1.7(2)	15.7(26)	43.4	3.66
106,779.0580 (60)	$9_{1,8} - 8_{2,7}$AE	0.5[h]	7.0	0.6(1)	15.7(26)	43.4	3.66
106,779.0660 (60)	$9_{1,8} - 8_{2,7}$EA	0.4[h]	7.0	0.4(1)	15.7(26)	43.4	3.66
		CH_3OH					
86,615.6020 (140)[e]	$7_{2,6} - 6_{3,3}$A−	6.3(4)	10.2(8)	5.8(4)	8.3(10)	102.7	1.36
86,902.9470 (140)[e]	$7_{2,5} - 6_{3,4}$A+	5.0(2)	8.9(6)	5.2(4)	8.9(8)	102.7	1.36
		^{13}CN					
108,631.1210 (1000)[d]	$N_{J,F} = 1_{1,0} - 0_{0,1}$	[i]	···	[i]	···	5.2	2.10
108,636.9230 (1000)[d]	$N_{J,F} = 1_{1,1} - 1_{0,1}$	[i]	···	[i]	···	5.2	2.10
108,638.2120 (1000)[d]	$N_{J,F} = 1_{1,1} - 0_{1,0}$	[i]	···	[i]	···	5.2	2.10

Table 4—Continued

Rest Frequency (MHz)[a]	Transition[b]	BIMA Array I_0 (Jy bm^{-1})	BIMA Array Δv (km s^{-1})	12 meter telescope I_0 (Jy bm^{-1})	12 meter telescope Δv (km s^{-1})	E_u (K)	$\langle S_{i,j}\mu^2 \rangle$ (D^2)
108,643.5900 (1000)[d]	$N_{J,F} = 1_{1,2} - 0_{1,1}$	[i]	···	[i]	···	5.2	2.10
108,645.0640 (2000)[d]	$N_{J,F} = 1_{1,1} - 0_{1,1}$	[i]	···	[i]	···	5.2	2.10
108,645.0640 (2000)[d]	$N_{J,F} = 1_{1,0} - 0_{1,1}$	[i]	···	[i]	···	5.2	2.10
108,651.2970 (1000)	$N_{J,F} = 1_{1,2} - 0_{0,1}$	[i]	···	[i]	···	5.2	2.10
108,657.6460 (1000)	$N_{J,F} = 1_{1,2} - 0_{1,2}$	[i]	···	[i]	···	5.2	2.10
108,658.9480 (1000)	$N_{J,F} = 1_{1,1} - 0_{1,2}$	[i]	···	[i]	···	5.2	2.10
108,780.2010 (1000)	$N_{J,F} = 1_{2,3} - 0_{1,2}$	[i]	···	[i]	···	5.2	4.21
108,782.3740 (1000)	$N_{J,F} = 1_{2,2} - 0_{1,1}$	[i]	···	[i]	···	5.2	4.21
108,786.9820 (1000)	$N_{J,F} = 1_{2,1} - 0_{1,0}$	[i]	···	[i]	···	5.2	4.21
108,793.7530 (1000)[d]	$N_{J,F} = 1_{2,1} - 0_{1,1}$	[i]	···	[i]	···	5.3	4.21
108,796.4000 (1000)[d]	$N_{J,F} = 1_{2,2} - 0_{1,2}$	[i]	···	[i]	···	5.3	4.21
		^{13}CO					
110,201.3700 (200)	$J = 1 - 0$	[i]	···	123.5(132)[j] 105.8(122)[j] 156.2(64)[j]	12.1(10) 10.8(6) 34.5(16)	5.3	0.01
		H$^{39}\alpha$					
106,737.3630	Recombination Line	< 0.4	···	4.0(2)	43.2(54)	···	···
		HC$_5$N					
106,498.9110 (80)	$J = 40 - 39$	< 0.4	···	1.7(2)	34.1(52)	103.6	749.96
		HC$_3$N					
109,990.0000 (2000)	$J = 12 - 11, \nu_6^1, \nu_7^1, \ell = 1e-$	1.3(2)	10.0(26)	< 0.6	···	1391.0	166.00[k]
110,050.7650 (184)	$J = 12 - 11, 3\nu_7^1, \ell = 1e$	3.1(4)	18.2(26)	1.6(6)	8.3(40)	990.7	165.27
		H^{13}CCCN					
106,474.1000 (10000)	$J = 12 - 11, \nu_7^2$	1.1(2)	33.0(116)	< 0.6	···	673.0	166.00[k]
		HC^{13}CCN					
108,710.5230 (240)	$J = 12 - 11$	3.5(2)	17.9(32)	6.9(4)	20.3(18)	33.9	166.42
		HCC^{13}CN					
108,721.0077 (144)	$J = 12 - 11$	4.6(4)	27.7(36)	8.1(4)	19.2(14)	33.9	166.42
		H^{13}CN					
86,338.7670 (600)	$J = 1 - 0\ F = 1 - 1$	[i]	···	[i]	···	4.0	8.91
86,340.1840 (600)	$J = 1 - 0\ F = 2 - 1$	[i]	···	[i]	···	4.0	8.91
86,342.2740 (600)	$J = 1 - 0\ F = 0 - 1$	[i]	···	[i]	···	4.0	8.91
		HC^{15}N					
86,054.9610 (600)	$J = 1 - 0$	[i]	···	[i]	···	4.1	8.91
		HCO					
	$N_{Ka,Kc} = 1_{0,1} - 0_{0,0}, J = \frac{3}{2} - \frac{1}{2}$						
86,670.8200 (800)	$F = 2 - 1$	< 0.3	···	2.8(4)	19.7(26)	4.2	1.86
86,708.3500 (800)	$F = 1 - 0$	< 0.3	···	2.1(2)	17.8(28)	4.2	1.86
		H^{13}CO$^+$					
86,754.3290 (780)	$J = 1 - 0$	[i]	···	[i]	···	4.2	10.89
		HC^{17}O$^+$					
87,057.5000 (10000)	$J = 1 - 0$	[i]	···	[i]	···	4.2	10.89
		HCOOCH$_3$ (MeF)					
85,919.0860 (280)	$7_{6,1} - 6_{6,0}$E	0.7(3)[l]	6.8(23)	< 0.6	···	40.4	5.00
85,926.5080 (220)	$7_{6,2} - 6_{6,1}$E	0.7(3)[l]	6.8(23)	< 0.6	···	40.4	5.00
85,927.2300 (240)	$7_{6,2} - 6_{6,1}$A	0.7(3)[l]	6.8(23)	< 0.6	···	40.4	5.00
85,927.2360 (240)	$7_{6,1} - 6_{6,0}$A	0.7(3)[l]	6.8(23)	< 0.6	···	40.4	5.00
86,021.0080 (260)	$7_{5,2} - 6_{5,1}$E	1.2(4)	5.6(22)	2.6(8)	3.6(12)	33.1	9.20
86,027.6740 (220)	$7_{5,3} - 6_{5,2}$E	1.5(4)	7.8(40)	1.2(6)	5.9(20)	33.1	9.20
86,029.4450 (240)	$7_{5,3} - 6_{5,2}$A	1.2(4)	4.2(28)	1.2(6)	5.9(20)	33.1	9.20
86,030.2120 (240)	$7_{5,2} - 6_{5,1}$A	1.8(6)	4.4(18)	1.2(8)	5.9(20)	33.1	9.20

Table 4—Continued

Rest Frequency (MHz)[a]	Transition[b]	BIMA Array I_0 (Jy bm^{-1})	BIMA Array Δv (km s^{-1})	12 meter telescope I_0 (Jy bm^{-1})	12 meter telescope Δv (km s^{-1})	E_u (K)	$\langle S_{i,j}\mu^2 \rangle$ (D^2)
86,210.0790 (240)	$7_{4,4} - 6_{4,3}$ A	1.3(2)	8.2(20)	1.7(4)	8.3[m]	27.2	12.70
86,223.5480 (260)	$7_{4,3} - 6_{4,2}$ E	1.5(2)	7.1(32)	1.2(6)	8.3[m]	27.2	12.60
86,224.1060 (220)	$7_{4,4} - 6_{4,3}$ E	1.3(2)	3.7(16)	1.7(4)	8.3[m]	27.2	12.60
86,250.5760 (240)	$7_{4,3} - 6_{4,2}$ A	1.5(2)	7.8(26)	3.1(4)	14.4(20)	27.2	12.70
86,265.8260 (240)	$7_{3,5} - 6_{3,4}$ A	1.7(4)	6.3(24)	2.9(4)	8.4(14)	22.4	15.30
86,268.6590 (220)	$7_{3,5} - 6_{3,4}$ E	1.3(4)	8.6(40)	2.5(4)	5.2(40)	22.6	15.20
90,145.6340 (240)	$7_{2,5} - 6_{2,4}$ E	2.0(2)	9.1(18)	2.3(4)	13.6(28)	19.7	17.30
90,156.5110 (260)	$7_{2,5} - 6_{2,4}$ A	1.9(2)	11.1(16)	3.3(6)	8.2(20)	19.7	17.30
90,227.5950 (260)	$8_{0,8} - 7_{0,7}$ E	2.2(4)	7.7(10)	2.8(30)	14.0(18)	20.1	21.00
90,229.6470 (280)	$8_{0,8} - 7_{0,7}$ A	2.2(4)	7.7(10)	3.0(26)	14.0(18)	20.0	21.00
			HCOOH				
86,546.1800 (200)	$4_{1,4} - 3_{1,3}$	0.5(2)	9.4(44)[h]	2.4(4)	10.8(44)	13.6	7.26
89,861.4800 (200)	$4_{2,3} - 3_{2,2}$	0.4(2)	14.1(48)	2.3(8)	8.5(33)[h]	23.5	5.80
89,948.2100 (200)[d]	$4_{3,2} - 3_{3,1}$	1.3(2)	9.2(36)	1.8(2)	7.2(14)	39.4	3.39
90,164.6200 (200)[d]	$4_{2,2} - 3_{2,1}$	0.9(2)	13.5(80)	1.9(4)	17.8(42)	23.5	5.80
			$HN^{13}C$				
87,090.7350 (920)	$J = 1 - 0$ $F = 0 - 1$	[i]	...	[i]	...	4.2	7.28
87,090.8590 (920)	$J = 1 - 0$ $F = 2 - 1$	[i]	...	[i]	...	4.2	7.28
87,090.9420 (920)	$J = 1 - 0$ $F = 1 - 1$	[i]	...	[i]	...	4.2	7.28
			HNCO				
109,905.7530 (100)[j]	$5_{0,5} - 4_{0,4}$	2.9(4) 1.7(12)	24.4(74) 6.3(56)	151.2(12) 23.6(22)	26.5(2) 6.8(8)	15.8	12.40
110,298.0980 (80)[h]	$5_{1,4} - 4_{1,3}$	8.5(8)	17.6(14)	8.4(6)	15.0(10)	59.0	11.91
			$HN^{13}CO$				
109908.8710 (440)[d]	$5_{0,5} - 4_{0,4}$	???	...	???	...	15.8	12.40
			NH_2CHO				
86,381.9540 (80)[d]	$7_{1,6} - 7_{0,7}$, $F = 7 - 7$	0.7[h]	7.5(40)	0.4[h]	7.2(56)	32.5	1.46[n]
86,383.2490 (30)[c,d]	$7_{1,6} - 7_{0,7}$, $F = 8 - 8$	1.5(6)	7.5(40)	1.6(6)	7.2(56)	32.5	1.69[n]
86,383.4350 (50)[c,d]	$7_{1,6} - 7_{0,7}$, $F = 6 - 6$	...	...	...	...	32.5	1.28[n]
106,541.8110 (800)	$5_{2,3} - 4_{2,2}$[e]	7.4(4)	12.5(8)	10.6(4)	17.8(6)	27.2	54.92
			NH_2D				
Ortho	$1_{0,1} - 1_{1,1}$						
85,924.7470 (400)	$F = 0 - 1$	0.1(0)	18.0(48)	0.3(0)	26.0(28)	20.7	0.36[n]
85,925.6840 (400)	$F = 2 - 1$	0.2(0)	18.0(48)	0.4(0)	26.0(28)	20.7	0.45[n]
85,926.2630 (200)	$F = 0 - 0$	0.0(0)	18.0(48)	0.0(0)	26.0(28)	20.7	0.00[n]
85,926.2630 (200)	$F = 1 - 1$	0.5(1)	18.0(48)	1.2(1)	26.0(28)	20.7	1.34[n]
85,926.2630 (200)	$F = 2 - 2$	0.1(0)	18.0(48)	0.2(0)	26.0(28)	20.7	0.27[n]
85,926.8580 (400)	$F = 1 - 2$	0.2(0)	18.0(48)	0.4(0)	26.0(28)	20.7	0.45[n]
85,927.7210 (400)	$F = 1 - 0$	0.1(0)	18.0(48)	0.3(0)	26.0(28)	20.7	0.36[n]
Para	$1_{0,1} - 1_{1,1}$						
110,152.0840 (400)	$F = 0 - 1$	0.5(2)	4.4(20)	0.7(3)	2.3(11)	21.2	0.36[n]
110,152.9950 (400)	$F = 2 - 1$	0.6(2)	4.4(20)	0.9(4)	2.3(11)	21.2	0.45[n]
110,153.5990 (200)	$F = 0 - 0$	0.0(0)	4.4(20)	0.0(0)	2.3(11)	21.2	0.00[n]
110,153.5990 (200)	$F = 1 - 1$	1.8(6)	4.4(20)	2.8(12)	2.3(11)	21.2	1.34[n]
110,153.5990 (200)	$F = 2 - 2$	0.3(1)	4.4(20)	0.5(2)	2.3(11)	21.2	0.27[n]
110,154.2220 (400)	$F = 1 - 2$	0.6(2)	4.4(20)	0.9(4)	2.3(11)	21.2	0.45[n]
110,155.0530 (400)	$F = 1 - 0$	0.5(2)	4.4(20)	0.7(3)	2.3(11)	21.2	0.36[n]
			$^{15}NNH^+$				
90,263.8330 (600)	$J = 1 - 0$	1.0(2)	6.3(20)	1.9(2)	14.2(28)	4.5	11.56
			$OC^{34}S$				
106,787.3800 (1600)	$J = 9 - 8$	3.8(10)	10.1(28)	4.8(4)	19.2(18)	26.3	4.60
			SiO				
86,846.8910 (560)	$J = 2 - 1$	[i]	...	[i]	...	6.3	19.20
			SO				
86,093.9380 (340)	$J_K = 2_2 - 1_1$[e]	7.6(4)	14.3(10)	19.8(2)	20.6(4)	19.3	3.60
			^{34}SO				

Table 4—Continued

Rest Frequency (MHz)[a]	Transition[b]	BIMA Array I_0 (Jy bm^{-1})	BIMA Array Δv (km s^{-1})	12 meter telescope I_0 (Jy bm^{-1})	12 meter telescope Δv (km s^{-1})	E_u (K)	$\langle S_{i,j}\mu^2 \rangle$ (D^2)
106,743.2440 (1400)	$J_N = 2_3 - 1_2$	1.2(6)	6.7(32)	2.0(8)	14.3(54)	20.9	3.63
			SO_2				
86,153.7090 (250)	$39_{9,31} - 40_{8,32}$	0.8(4)	4.0(26)	< 0.6	···	916.1	15.91
86,639.0400 (1000)	$8_{3,5} - 9_{2,8}$	2.0(2)	20.7(38)	1.5(4)	13.0(34)	55.2	3.02
86,828.8820 (590)[d]	$20_{2,18} - 21_{1,21}$	< 0.2	···	1.9[h]	6.8	207.8	0.07

[a]Uncertainty is 95% (2σ) confidence level.

[b]Transitions are J_{K_a,K_c} unless otherwise noted.

[c]These transitions were blended and were fit with a single Gaussian.

[d]Previously undetected transition.

[e]Multiple emission components are visible. Only the intensity and line width of the main component are given.

[f] For EtOH a "+"=gauche+ and a "-"=gauche- state.

[g]These transitions were highly blended and thus the intensity and line widths were approximated because the least squares Gaussian fitting did not give a satisfactory fit.

[h]Intensity and line width were approximated because the least squares Gaussian fitting did not give a satisfactory fit.

[i]Multiple emission and absorption components detected.

[j]Multiple strong components are apparent in the data (see Figure 2), each component is listed on a separate line in this table.

[k]Estimated value since the dipole moment μ was not stated in the reference.

[l]Due to confusion from transitions from NH_2D the intensity and line width of this transition of MeF was extrapolated from the other detected MeF transitions.

[m]Line width was fixed in order to get an adequate intensity fit.

[n]In order to calculate the line strength of these hyperfine components the line strength for the entire transition was multiplied by the relative intensity of the hyperfine component.

Table 5. Detected Unidentified Lines

Rest Frequency (MHz)	BIMA Array I_0 (Jy bm^{-1})	BIMA Array Δv (km s^{-1})	12 meter telescope I_0 (Jy bm^{-1})	12 meter telescope Δv (km s^{-1})	Potential Identification Transition, Frequency(MHz) and Species)
85,907.7[a]	0.7[b]	3.4	< 0.6	···	
85,910.5	1.0(4)	10.9(68)	< 0.6	···	$9_{4,6} - 8_{4,5}$, 85,910.564, C_2H_3CN $\nu2$=11(FJL)
					$9_{4,5} - 8_{4,4}$, 85,910.632, C_2H_3CN $\nu2$=11(FJL)
85,912.7[a]	0.9[b]	1.7	< 0.6	···	
85,917.5	0.9(4)	6.9(36)	< 0.6	···	$9_{6,*} - 8_{6,*}$, 85,917.187, C_2H_3CN $\nu2$=11(FJL)
85,932.7[a]	< 0.3	···	1.2(6)	3.9(28)	
85,935.1	1.0(4)	6.9(28)	2.1(4)	6.9(20)	
85,939.1	0.7(2)	10.5(54)	< 0.6	···	
85,942.0[a]	< 0.3	···	-4.2(8)	3.1(6)	
85,945.9	0.9(4)	5.0(26)	< 0.6	···	$9_{8,*} - 8_{8,*}$, 85,945.968, C_2H_3CN $\nu2$=11(FJL)
85,970.6[a]	0.7(6)	3.3(30)	< 0.6	···	
85,973.2	0.4[b]	5.7	< 0.6	···	$13_{2,12} - 12_{3,9}$AA, 85,973.249, $(CH_3)_2O$(Groner et al. 1998)
85,987.4	1.9(4)	10.5(24)	< 0.6	···	$9_{2,7} - 8_{2,6}$, 85,987.176, C_2H_3CN $\nu1$=11(FJL)
86,010.0	0.8(4)	5.1(32)	< 0.6	···	
86,024.3[a]	< 0.3	···	4.1(8)	2.7(6)	
86,034.3	0.8(4)	5.1(32)	< 0.6	···	
86,133.2	0.5(2)	10.0(72)	< 0.6	···	$18^+_{4,14} - 18^-_{3,16}$;[c] 86,132.920, EtOH(JCP)
					$6_{3,3} - 6_{3,4}$ $J = 11/2 - 11/2$, 86,129.608-86,133.000;[d] c-$CC^{13}CH$(Pickett et al. 1998)
86,148.0	0.5(4)	5.3(48)	< 0.6	···	$6_{3,3} - 6_{3,4}$ $J = 11/2 - 11/2$, 86,147.719-86150.854;[d] c-$CC^{13}CH$(Pickett et al. 1998)
86,151.6	0.6(2)	17.3(140)	< 0.6	···	
86,204.6	0.9(2)	5.4(20)	< 0.6	···	
86,207.8	0.9(2)	7.4(28)	< 0.6	···	
86,220.9	0.9(2)	4.7(24)	2.1(4)	14.9(40)	
86,226.5	0.7(2)	13.2(74)	< 0.6	···	$2_{2,0} - 2_{1,1}$EE, 86,226.727, $(CH_3)_2O$(Groner et al. 1998)
86,239.6	< 0.2	···	1.7(4)	8.1(34)	
86,243.5	< 0.2	···	1.6(4)	10.6(46)	$2 - 1, \nu = 1$, 86,243.440, SiO[e](Lovas 2004; Snyder & Buhl 1974)
86,248.2	0.8(2)	6.6(34)	< 0.6	···	
86,255.2	0.6(2)	12.2(54)	< 0.6	···	$9_{2,7} - 8_{2,6}$, 86,254.848, C_2H_3CN $\nu2$=11(FJL)
86,263.5	< 0.2	···	1.4(4)	10.0(56)	
86,297.2	0.4(2)	5.0(38)	< 0.6	···	
86,300.7	0.7(2)	12.5(40)	< 0.6	···	$29 - 28$, 86,300.430, $^{30}SiC_4$(FJL)
86,386.3	0.9(4)	4.6(24)	< 0.6	···	
86,389.2	-1.1(4)	2.2(12)	-2.7(8)	2.4(8)	
86,395.9[f]	0.9(2)	5.2(18)	1.9(6)	3.3(14)	
86,398.8	0.8(2)	7.4(26)	< 0.6	···	
86,421.8	0.6(2)	6.7(32)	< 0.6	···	
86,436.5[a]	0.6(4)	1.9(12)	< 0.6	···	
86,440.2	0.5(2)	17.8(76)	< 0.6	···	
86,445.8	0.6(2)	9.9(46)	< 0.6	···	
86,459.3	0.5(4)	5.2(46)	< 0.6	···	$6_{3,3} - 6_{3,4}$ $J = 13/2 - 13/2$, 86,458.768-86,459.831;[d] c-$CC^{13}CH$(Pickett et al. 1998)
86,473.4[f]	0.7(2)	8.9(26)	< 0.6	···	
86,486.6	0.6[b]	3.2	1.3(2)	24.2(72)	
86,498.2[a]	0.7[b]	1.9	< 0.6	···	
86,536.6	0.6(2)	4.8(28)	< 0.6	···	
86,543.7	< 0.2	···	2.4(6)	8.3(30)	
86,784.5	-1.4(6)	3.7(20)	-2.2(8)	3.8(14)	
86,794.5	< 0.3	···	-1.4(4)	5.1(20)	
86,803.6	-1.2(6)	2.2(18)	-2.0(8)	2.2(12)	
86,812.3	< 0.3	···	1.6(2)	10.7(34)	
86,831.6	0.8[b]	2.5	1.7[b]	6.0	$13_3 - 14_2$A+, 86,831.480, CH_3SH(FJL)
86,915.5	0.8(2)	9.5(30)	< 0.6	···	
86,944.5[a]	1.0(4)	3.7(20)	< 0.6	···	
86,956.1[a]	0.7(2)	3.6(12)	< 0.6	···	
86,957.8[a]	0.8(2)	2.2(10)	< 0.6	···	
86,976.0	1.3(4)	4.4(16)	1.5(6)	3.9(20)	
86,979.3[f]	1.9(2)	9.5(18)	1.6(4)	10.1(32)	$10_{1,10} - 9_{1,9}$A, 86,978.865, EtCN(JCP)
					$10_{1,9} - 9_{1,8}$E, 86,978.884, EtCN(JCP)
87,008.3	0.5(2)	14.5(40)	< 0.6	···	
87,016.5	0.5(2)	8.5(28)	< 0.6	···	$4_{3,2} - 3_{3,1}$, 87,016.896, HCOOD(Pickett et al. 1998)
87,027.4	0.7(2)	6.7(24)	< 0.6	···	$5^-_{2,3} - 4^-_{2,2}$;[c] 87,027.093, EtOH(JCP)
89,731.9	0.9(4)	7.1(36)	< 0.7	···	
89,739.6	4.1(2)	22.6(20)	2.9(4)	15.7(22)	$10_{4,6} - 9_{4,5}$A, 89,739.381, EtCN(JCP)
					$10_{4,6} - 9_{4,5}$E, 89,739.935, EtCN(JCP)
89,754.9	1.6(8)	4.8(26)	1.2(6)	5.3(32)	
89,767.3	1.7(2)	32.6(54)	< 0.7	···	
89,791.5	0.6(2)	18.4(82)	< 0.7	···	
89,814.7	0.8(2)	11.9(40)	1.1(4)	8.8(32)	$33_{1,32} - 33_{1,33}$, 89,814.7342-89,816.2485;[g] HNCO(Pickett et al. 1998)
89,829.6	0.8(4)	5.9(26)	< 0.7	···	
89,897.3	0.3(2)	15.4(14)	< 0.7	···	
89,902.3	0.5(4)	5.4(42)	< 0.7	···	
89,923.8	0.4(2)	9.1(60)	< 0.7	···	
89,959.4[a]	0.8(4)	3.4(20)	< 0.7	···	
89,989.7	0.8(2)	10.3(36)	< 0.7	···	
89,993.1	0.8(2)	7.5(26)	< 0.7	···	$33_{1,32} - 33_{1,33}$, 89,992.9883-89,993.4035;[g] $HN^{13}CO$(Pickett et al. 1998)
90,004.8	0.6(2)	5.5(30)	< 0.7	···	
90,007.7	0.7(2)	8.8(38)	< 0.7	···	$13^+_{0,13} - 13^+_{1,13}$;[c] 90,007.693, EtOH(JCP)
90,033.9	1.0(2)	11.6(50)	< 0.7	···	

Table 5—Continued

Rest Frequency (MHz)	BIMA Array I_0 (Jy bm^{-1})	BIMA Array Δv (km s^{-1})	12 meter telescope I_0 (Jy bm^{-1})	12 meter telescope Δv (km s^{-1})	Potential Identification Transition, Frequency(MHz) and Species)
90,037.8[f]	1.7(2)	12.1(40)	2.2(4)	8.2(20)	
90,069.1	0.5(2)	6.3(34)	< 0.7	···	
90,078.3	0.8(2)	18.5(38)	< 0.7	···	$17_{2,15} - 17_{2,16}$, 90,077.914, HCOOH(Pickett et al. 1998)
90,128.5	0.5(2)	4.8(32)	< 0.7	···	
90,142.9	0.8(4)	4.1(26)	< 0.7	···	
90,153.8	< 0.2	···	2.3(6)	5.3(22)	
90,166.9	1.2(6)	6.8(32)	< 0.7	···	
90,174.5	0.6(2)	11.8(62)	< 0.7	···	
90,179.1	0.7(2)	7.4(36)	< 0.7	···	$24^+_{4,21} - 23^-_{5,19}$;[c] 91,178.955, EtOH(JCP)
90,203.4[f]	0.7(2)	13.2(36)	< 0.7	···	
90,224.5	1.3(4)	1.6(6)	2.2(8)	2.2(10)	
90,304.8	0.6(4)	4.1(34)	< 0.7	···	
90,307.9	0.6(2)	12.0(66)	< 0.7	···	$23_{3,21} - 22_{4,19}$, 90,307.778, C_2H_5OOCH(Pickett et al. 1998)
106,295.4	1.0(4)	9.1(56)	< 0.6	···	
106,322.0	1.0(2)	22.9(84)	< 0.6	···	$18^+_{2,16} - 18^+_{1,17}$;[c] 106,322.066, EtOH(JCP)
106,353.0	0.9(2)	17.3(66)	< 0.6	···	$22_{3,19} - 21_{4,18}$, 106,352.655-106,353.379;[d] $SO^{17}O$(FJL)
					$32_{3,29} - 33_{2,32}$, 106,351.742-106,353.062;[d] $SO^{17}O$(FJL)
					$11_{1,10} - 10_{2,9}$, 106,352.528-106,352.878;[d] DNO(Pickett et al. 1998)
106,371.5[a]	1.9(6)	3.9(16)	< 0.6	···	
106,411.6	1.4(4)	7.3(30)	< 0.6	···	$5_{2,3} - 4_{2,2}$, 106,411.010-106,411.461;[d] $NH_2^{13}CHO$(FJL)
					$35_{22,14} - 35_{21,15}$AA, 106,411.273, $(CH_3)_2CO$ (Groner et al. 2002; Snyder et al. 2002)
106,448.9	3.4(4)	7.7(14)	1.8(6)	5.5(20)	
106,468.5	0.8(6)	10.6(74)	< 0.6	···	
106,484.8[a]	1.5(8)	1.9(10)	< 0.6	···	$5_{1,5} - 4_{1,4}$, 106,484.610, $HO^{13}CO^+$(Pickett et al. 1998)
					$15^-_{6,10} - 16^+_{5,12}$;[c] 106,484.991, EtOH(JCP)
106,487.2	1.1(2)	13.9(46)	< 0.6	···	
106,510.7	1.5(4)	5.7(22)	< 0.6	···	
106,514.5	1.8(4)	5.9(18)	< 0.6	···	
106,559.8	0.9(4)	5.8(38)	< 0.6	···	
106,629.9	1.2(4)	6.6(30)	< 0.6	···	
106,638.4	4.3(18)	6.6(24)	4.0(8)	6.6(14)	$4_5 - 3_4$, 106,638.559, $HC_2^{15}N$(FJL)
					$11_{2,12} - 10_{2,11}$, 106,638.577, C_4H(Müller et al. 2001)
106,654.8	2.8(4)	6.4(14)	1.7(4)	12.2(42)	
106,706.7	1.2(6)	5.4(32)	< 0.6	···	
106,714.3	1.0(6)	4.5(36)	< 0.6	···	
106,753.1	1.5(4)	8.8(26)	2.2(6)	6.1(18)	$11_{1,10} - 10_{1,9}$ vt=2, 106,753.070, C_2H_3CN(Pickett et al. 1998)
106,763.3[a]	1.3(8)	2.2(16)	< 0.6	···	
106,767.4	1.0(4)	5.2(28)	< 0.6	···	$6^-_{1,5} - 5^-_{1,4}$;[c] 106,767.176, EtOH(JCP)
108,207.3	1.8(16)	4.3(46)	< 0.9	···	$2_{2,0} - 3_{1,3}$, 108,207.399, VyCN(Pickett et al. 1998)
108,223.7[a]	2.1(14)	3.9(32)	< 0.9	···	
108,379.8	1.9(12)	3.5(24)	2.3(6)	6.6(20)	
108,434.9	1.6(4)	5.0(12)	1.6(8)	7.7(40)	$14_{2,12} - 14_{1,13}$EE, 108,434.511, $(CH_3)_2CO$(Groner et al. 2002; Snyder et al. 2002)
					$26 - 25$, $J = 49/2 - 49/2$, 108,435.7053, l-HC_4N(Müller et al. 2001)
108,507.7	1.3(4)	9.1(68)	< 0.9	···	
108,511.2	1.3(6)	7.4(62)	< 0.9	···	$31_{3,29} - 30_{4,26}$, 108,511.262-108,511.299;[d] $^{33}SO_2$(Müller et al. 2001)
108,620.7[a]	2.2(8)	1.8(10)	< 0.9	···	
109,943.3	2.0(4)	5.0(16)	< 0.6	···	
109,959.6	3.5(4)	10.5(16)	2.1(6)	8.1(44)	$33_{1,33} - 34_{0,34}$, 109,959.100, HNCO(Winnewisser, Hocking, & Gerry 1976)
					$22_{1,21} - 22_{1,22}$, 109,958.699, EtCN(Lovas 1982)
					$16_{8,9} - 15_{8,8}$, 109,960.360, NH_2CH_2COOH-I (glycine)[h](FJL)
109,972.0	0.9(6)	4.1(30)	< 0.6	···	
110,028.6[a]	< 0.5	···	2.4(16)	1.3(10)	
110,036.2	3.5[b]	3.3	1.5(8)	5.9(36)	
110,079.7	0.9(4)	6.7(40)	< 0.6	···	
110,085.6	2.0(4)	13.3(38)	1.9(8)	6.3(26)	$4_{2,3} - 3_{1,2}$A vt=1, 110,085.727, EtCN(JCP)
110,090.2	1.2(6)	4.7(28)	< 0.6	···	$6_{5,2} - 5_{4,1}$AE, 110,089.569, $(CH_3)_2CO$(Groner et al. 2002; Snyder et al. 2002)
					$7_{5,3} - 6_{4,2}$, 110,089.998, NH_2CH_2COOH-I[i](FJL)
					$4_{2,2} - 3_{1,3}$E vt=1, 110,090.695, EtCN(JCP)
110,098.0	1.2(4)	10.8(28)	< 0.6	···	
110,104.7	1.7(4)	10.8(38)	< 0.6	···	$4_{4,0} - 3_{2,1}$, 110,104.847, NH_2CH_2COOH-I[i](FJL)
110,143.3	2.5[b]	16.7	< 0.6	···	
110,150.0	2.2(6)	7.8(26)	< 0.6	···	$9_{2,7} - 8_{3,6}$EA, 110,149.102, $(CH_3)_2CO$(Groner et al. 2002; Snyder et al. 2002)
					$9_{2,7} - 8_{3,6}$AE, 110,148.838, $(CH_3)_2CO$(Groner et al. 2002; Snyder et al. 2002)
110,158.2	< 1.0	···	5.1[j]	31.8	$26_{21,6} - 26_{20,7}$EA, 110,158.590, $(CH_3)_2CO$(Groner et al. 2002; Snyder et al. 2002)
			3.6[j]	1.9	
110,161.0[a]	< 1.0	···	3.5(14)	2.6(12)	
110,164.6[a]	< 1.0	···	4.5(12)	3.1(12)	$5_{1,4} - 4_{1,3}$, 110,164.245, HNCO ν_6[k](Lovas 2004; Wyrowski, Schilke, & Walmsley 1999)
110,213.0	[l]	···	[l]	···	
110,216.4	< 0.8	···	[l]	···	$5_{4,1} - 4_{4,0}$, 110,216.85, DCOOH(Willemot et al. 1980)
					$5_{4,2} - 4_{4,1}$, 110,216.64, DCOOH(Willemot et al. 1980)
110,222.2	[l]	···	[l]	···	
110,233.6	[l]	···	[l]	···	
110,239.9[f]	[l]	···	[l]	···	
110,246.6	< 0.8	···	[l]	···	
110,253.0	[l]	···	< 0.6	···	$15_{15} - 14_{14}$, 110,252.932, $C^{13}CS$(Pickett et al. 1998)
110,255.5	< 0.5	···	[l]	···	$4_{4,1} - 5_{3,2}$AA, 110,256.338, $(CH_3)_2O$(Groner et al. 1998)
110,263.8	[l]	···	[l]	···	

Table 5—Continued

Rest Frequency (MHz)	BIMA Array I_0 (Jy bm^{-1})	BIMA Array Δv (km s^{-1})	12 meter telescope I_0 (Jy bm^{-1})	12 meter telescope Δv (km s^{-1})	Potential Identification Transition, Frequency(MHz) and Species)
110,418.4	2.9(10)	9.4(46)	< 0.6	···	$22_{20,2} - 22_{19,3}$EA, 110,417.969, $(CH_3)_2CO$(Groner et al. 2002; Snyder et al. 2002)
110,421.4[a]	2.8(18)	2.9(24)	< 0.6	···	$36 - 35$, 110,420.724, SiC_4(Pickett et al. 1998)
110,446.8	2.6(8)	6.4(26)	< 0.6	···	$9_{8,1} - 8_{8,0}$E, 110,447.032, MeF(Oesterling et al. 1999)
110,447.9	< 0.97	···	2.6(10)	4.9(20)	$14_{3,12} - 14_{2,13}$A, 110,447.595, EtCN(JCP)

[a]This feature is a questionable detection because its line width is <4 km s^{-1}; hence it may be due to interference.

[b]Intensity and line width were approximated because the least squares Gaussian fitting did not give a satisfactory fit.

[c]For EtOH a "+"= gauche+ and a "-"= gauche- states.

[d]Large frequency spread due to hyperfine components.

[e]The transition has been previously reported as a masing transition in Orion by Snyder & Buhl (1974). However due to its large line width combined with its very high E_u ($\sim$1760 K) it is unlikely that this identification is correct for this source.

[f]Previously detected U line.

[g]Large frequency spread due to multiple J components.

[h]It is not likely that this line is from glycine since it is detected strongly with both instruments and glycine is expected to be very compact in distribution.

[i]It is not likely that this line is from glycine since this transition has an unfavorable line strength.

[j]Multiple components were necessary to get an approximate least squares Gaussian fit. Each component is listed on a separate line.

[k]This transition has been previously reported as a HNCO transition toward G10.47+0.03 by Wyrowski, Schilke, & Walmsley (1999). However due to its narrow line width we are reporting it as a questionable detection for Sgr B2(N-LMH).

[l]Multiple emission and absorption components detected.

Table 6. Comparison of Line Statistics

	Identified		Unidentified		Total	
Source	Lines	Density[a]	Lines	Density[a]	Lines	Density[a]
Cummins, Thaddeus, & Linke (1986)	49	1.36	3	0.08	52	1.44
Turner (1989)	57	1.58	10	0.28	67	1.86
Lovas (2004)	151	4.19	38	1.06	189	5.25
This survey	98	2.72	120	3.34	218	6.06

[a]Lines per 100 MHz.